arXiv:1602.02229v1 [cond-mat.str-el] 6 Feb 2016

Basic Properties of Conductivity and Normal Hall Effect in the Periodic Anderson Model

Shinji Watanabe[1] and Kazumasa Miyake[2]

[1]*Department of Basic Sciences, Kyushu Institute of Technology, Kitakyushu, Fukuoka 804-8550, Japan*
[2]*Toyota Physical and Chemical Research Institute, Nagakute, Aichi 480-1192, Japan*

Exact formulas of diagonal conductivity σ_{xx} and Hall conductivity σ_{xy} are derived from the Kubo formula in hybridized two-orbital systems with arbitrary band dispersions. On the basis of the theoretical framework for the Fermi liquid based on these formulas, the ground-state properties of the periodic Anderson model with electron correlation and weak impurity scattering are studied on the square lattice. It is shown that imbalance of the mass-renormalization factors in σ_{xx} and σ_{xy} causes remarkable increase in the valence-fluctuation regime as the f level increases while the cancellation of the renormalization factors causes slight increase in σ_{xx} and σ_{xy} in the Kondo regime. The Hall coefficient $R_{\rm H}$ shows almost constant behavior in both the regimes. Near half filling, $R_{\rm H}$ is expressed by the total hole density as $R_{\rm H} = 1/(\tilde{n}_{\rm hole}e)$ while $R_{\rm H}$ approaches zero near quarter filling, which reflects the curvature of the Fermi surface. These results hold as far as the damping rate for f electrons is less than about 10 % of the renormalized hybridization gap. From these results we discuss pressure dependence of residual resistivity and normal Hall effect in Ce- and Yb-based heavy electron systems.

1. Introduction

The heavy-electron systems have attracted much attention in condensed matter physics since the localized and itinerant natures of strongly correlated electrons open up unexpected phenomena, which leads to a break through the paradigm to provide a new concept with universality. The emergence of the heavy mass of quasiparticles, their condensation to the superconductivity with essentially "high" transition temperature compared to the renormalized Fermi temperature, and unconventional quantum critical phenomena[1,2] are such examples.

To make experimental explorations, the measurements of the conductivity and Hall effect have been performed extensively in the heavy-electron systems. Accumulated data for the Ce-based heavy electron systems show that there exists a general tendency that the isothermal resistivity at the measured lowest temperature, i.e., residual resistivity, in the Fermi-liquid regime decreases as pressure increases.[3–5] On the other hand, in the Yb-based heavy-electron systems, there exits a general tendency that the residual resistivity in the Fermi-liquid regime increases as pressure increases.[6–11] The mechanism of the pressure dependence of the conductivity and also the Hall conductivity in relation to the valence of Ce and Yb as well as the shape of the Fermi surface has been desired to be clarified theoretically.

Theoretically, the diagonal conductivity and the Hall conductivity were formulated on the basis of the Boltzmann transport theory.[12–14] The formula of the diagonal conductivity in the system with Coulomb repulsion among electrons was derived microscopically by Éliashberg[16] in the Fermi liquid theory starting from the Kubo formula.[15] The diagonal conductivity in the periodic Anderson model which is the prototypical model for the Ce- and Yb-based heavy electron systems was formulated on the basis of the Fermi liquid theory by Yamada and Yosida.[17]

The Hall conductivity was formulated by Fukuyama[18,19] in the gauge invariant manner starting from the Kubo formula. Later, Éliashberg's work was extended to the Hall conductivity by Kohno and Yamada, who formulated the general expression in the Femi liquid theory.[20] Explicit calculation of the diagonal and Hall conductivities was performed by using the conserving approximation[21–23] in the Hubbard model which contains a single orbital with electron transfer and Coulomb repulsion by Kontani *et al*.[24]

So far, after the formulation of the diagonal conductivity by Yamada and Yosida, systematic calculations for the diagonal and normal Hall conductivities have not been reported in detail in the periodic Anderson model which contains the two orbitals for f and conduction electrons.

In this paper, we clarify the basic properties of the diagonal and Hall conductivities, and normal Hall effect in the periodic Anderson model. On the basis of the theoretical framework which describes the Fermi liquid correctly, the ground-state properties of the diagonal and Hall conductivities and the Hall coefficient are studied by taking into account the effects of the electron correlation and the weak impurity scattering. By performing the numerical calculation on the square lattice, the dependence on parameters such as the f level, c-f hybridization, the damping rate for f electrons, and the filling is clarified. The relation to the shape of the Fermi surface and the f-electron number per site, corresponding to the valence of Ce and Yb, is also clarified.

The organization of this paper is as follows: In Sect. 2, we review the formalism of conductivity in the periodic Anderson model based on the Fermi-liquid theory. In Sect. 3, exact formulas of the diagonal conductivity and Hall conductivity are derived in the periodic Anderson model for $U = 0$. In Sect. 4, the ground-state properties of the conductivities and the Hall coefficient in the periodic Anderson model with electron correlations and weak-impurity scattering are studied on the basis of the exactly derived formulas. The paper is summarized in Sect. 5.

We take the energy units as $\hbar = 1$, $k_{\rm B} = 1$, and the light velocity $c = 1$. Note that we denote e as the elementary charge, i.e., $e > 0$.

2. Formalism of conductivity based on the Fermi liquid theory in the periodic Anderson model

As the simplest minimal model for the electronic state in the Ce- and Yb-based heavy-electron systems, we consider the periodic Anderson model

$$\mathcal{H} = \sum_{\mathbf{k}\sigma} \varepsilon_{\mathbf{k}} c^{\dagger}_{\mathbf{k}\sigma} c_{\mathbf{k}\sigma} + \sum_{\mathbf{k}\sigma} \varepsilon^{\mathrm{f}}_{\mathbf{k}} f^{\dagger}_{\mathbf{k}\sigma} f_{\mathbf{k}\sigma} + \sum_{\mathbf{k}\sigma} V_{\mathbf{k}} \left(f^{\dagger}_{\mathbf{k}\sigma} c_{\mathbf{k}\sigma} + c^{\dagger}_{\mathbf{k}\sigma} f_{\mathbf{k}\sigma} \right) + U \sum_{i} n^{\mathrm{f}}_{i\uparrow} n^{\mathrm{f}}_{i\downarrow}, \quad (1)$$

with $n^{\mathrm{f}}_{i\sigma} \equiv f^{\dagger}_{i\sigma} f_{i\sigma}$ where $f_{i\sigma}$ ($f^{\dagger}_{i\sigma}$) is an annihilation (creation) operator of an f electron at the i-th site with spin σ and $c_{\mathbf{k}\sigma}$ ($c^{\dagger}_{\mathbf{k}\sigma}$) is an annihilation (creation) operator of a conduction electron at the wave vector $\mathbf{k}$ with spin σ. The first term represents the energy band of conduction electrons with a dispersion, $\varepsilon_{\mathbf{k}}$. The second term represents the energy of f electrons allowed to have a dispersion, $\varepsilon^{\mathrm{f}}_{\mathbf{k}}$, which we here consider for generality. The third term represents the hybridization between f and conduction electrons with real $V_{\mathbf{k}}$. The on-site Coulomb repulsion for f electrons is expressed in the last term.

Since $4f^1 5d^1 6s^2$ configuration is realized in the outermost electrons' shell of Ce, Ce^{+3} contains the $4f^1$ electron and Ce^{+4} contains the $4f^0$ electron. On the other hand, since $4f^{14} 6s^2$ configuration is realized in the outermost electrons' shell of Yb, Yb^{3+} contains the $4f^{13}$ electrons and Yb^{2+} contains $4f^{14}$ electrons. Since $4f^{14}$ is the closed shell for the f orbital, by taking the hole picture instead of the electron picture, Eq. (1) can be applied to the Yb-based systems and the parallel discussion to the Ce-based systems in the electron picture can be made.

The total filling $\bar{n}$ is defined as

$$\bar{n} \equiv n_{\mathrm{f}} + n_{\mathrm{c}}, \quad (2)$$

where n_{f} and n_{c} are f-electron number per site and the conduction electron number per site, respectively, defined as

$$n_{\mathrm{f}} = \frac{1}{N} \sum_{i\sigma} \langle n^{\mathrm{f}}_{i\sigma} \rangle, \quad (3)$$

$$n_{\mathrm{c}} = \frac{1}{N} \sum_{i\sigma} \langle n^{\mathrm{c}}_{i\sigma} \rangle. \quad (4)$$

Here, N is the number of the lattice sites and $n^{\mathrm{c}}_{i\sigma} \equiv c^{\dagger}_{i\sigma} c_{i\sigma}$. Note that $\bar{n} = 2$ is the half filling.

The diagonal conductivity in the periodic Anderson model was formulated on the basis of the Fermi liquid theory by Yamada and Yosida.[17] In the following, we review the formalism for the diagonal conductivity.

The retarded Green functions of f electrons and conduction electrons are given by

$$G^{\mathrm{ff\,R}}_{\mathbf{k}}(\varepsilon) = \left[\varepsilon + i\delta - \varepsilon^{\mathrm{f}}_{\mathbf{k}} - \Sigma^{\mathrm{R}}_{\mathbf{k}}(\varepsilon) - \frac{V^2_{\mathbf{k}}}{\varepsilon + i\delta - \varepsilon_{\mathbf{k}}} \right]^{-1}, \quad (5)$$

$$G^{\mathrm{cc\,R}}_{\mathbf{k}}(\varepsilon) = \left[\varepsilon + i\delta - \varepsilon_{\mathbf{k}} - \frac{V^2_{\mathbf{k}}}{\varepsilon + i\delta - \varepsilon^{\mathrm{f}}_{\mathbf{k}} - \Sigma^{\mathrm{R}}_{\mathbf{k}}(\varepsilon)} \right]^{-1}, \quad (6)$$

respectively, where $\Sigma^{\mathrm{R}}_{\mathbf{k}}(\varepsilon)$ is the retarded self energy of f electrons, which arises from the Coulomb repulsion U, and δ is the infinitesimal positive constant.

We consider the case where the Fermi level is located at the lower hybridized band. In the vicinity of the Fermi energy, the Green functions of f and conduction electrons are described by quasiparticles as

$$G^{\mathrm{ffR}}_{\mathbf{k}}(\varepsilon) = a^{\mathrm{ff}}_{-,\mathbf{k}} G^{\mathrm{ff-R}}_{\mathbf{k}}(\varepsilon), \quad (7)$$

$$G^{\mathrm{ccR}}_{\mathbf{k}}(\varepsilon) = a^{\mathrm{cc}}_{-,\mathbf{k}} G^{\mathrm{ff-R}}_{\mathbf{k}}(\varepsilon), \quad (8)$$

respectively, where the retarded Green function for the lower hybridized band is given by

$$G^{\mathrm{ff-R}}_{\mathbf{k}}(\varepsilon) = \frac{1}{\varepsilon - E^{-*}_{\mathbf{k}} + i\Gamma^{*}_{\mathbf{k}}} \quad (9)$$

and the renormalization factors are given by

$$a^{\mathrm{ff}}_{-,\mathbf{k}} = \left[1 - \frac{\partial \mathrm{Re}\Sigma^{\mathrm{R}}_{\mathbf{k}}(\varepsilon)}{\partial \varepsilon} + \frac{V^2_{\mathbf{k}}}{(\varepsilon - \varepsilon_{\mathbf{k}})^2} \right]^{-1} \Bigg|_{\varepsilon = E^{-*}_{\mathbf{k}}}, \quad (10)$$

$$a^{\mathrm{cc}}_{-,\mathbf{k}} = \left(\frac{V_{\mathbf{k}}}{E^{-*}_{\mathbf{k}} - \varepsilon_{\mathbf{k}}} \right)^2 a^{\mathrm{ff}}_{-,\mathbf{k}}, \quad (11)$$

respectively. Here, the renormalized lower hybridized band is given by

$$E^{-*}_{\mathbf{k}} = \frac{\varepsilon_{\mathbf{k}} + \tilde{\varepsilon}^{\mathrm{f}}_{\mathbf{k}}}{2} - \frac{1}{2} \sqrt{\left(\varepsilon_{\mathbf{k}} - \tilde{\varepsilon}^{\mathrm{f}}_{\mathbf{k}} \right)^2 + 4\tilde{V}^2_{\mathbf{k}}} \quad (12)$$

with the renormalized f level

$$\tilde{\varepsilon}^{\mathrm{f}}_{\mathbf{k}} \equiv z_{\mathbf{k}} \left[\varepsilon^{\mathrm{f}}_{\mathbf{k}} + \mathrm{Re}\Sigma^{\mathrm{R}}_{\mathbf{k}}(\mu) \right], \quad (13)$$

and the renormalized hybridization $\tilde{V}^2_{\mathbf{k}} \equiv z_{\mathbf{k}} V^2_{\mathbf{k}}$. Here, $z_{\mathbf{k}}$ is defined as

$$z_{\mathbf{k}} \equiv \left[1 - \frac{\partial \mathrm{Re}\Sigma^{\mathrm{R}}_{\mathbf{k}}(\varepsilon)}{\partial \varepsilon} \right]^{-1} \Bigg|_{\varepsilon = \mu}, \quad (14)$$

and μ is the chemical potential. The renormalized damping rate is given by

$$\Gamma^{*}_{\mathbf{k}} = a^{\mathrm{ff}}_{-,\mathbf{k}} \left(-\mathrm{Im}\Sigma^{\mathrm{R}}_{\mathbf{k}}(\mu) \right) > 0. \quad (15)$$

The diagonal conductivity is expressed as

$$\sigma_{xx} = \frac{e^2}{V_0} \sum_{\mathbf{k}} \int_{-\infty}^{\infty} \frac{d\varepsilon}{\pi} \left(-\frac{\partial f(\varepsilon)}{\partial \varepsilon} \right) \left\{ \left| G^{\mathrm{ff\,R}}_{\mathbf{k}}(\varepsilon) \right|^2 v_{\mathbf{k}x}(\varepsilon) J_{\mathbf{k}x}(\varepsilon) - \mathrm{Re}\left[G^{\mathrm{ff\,R}^2}_{\mathbf{k}}(\varepsilon) v^2_{\mathbf{k}x}(\varepsilon) \right] \right\}, \quad (16)$$

where $f(\varepsilon)$ is the Fermi distribution function $f(\varepsilon) = [\mathrm{e}^{(\varepsilon-\mu)/T} + 1]^{-1}$ and $G^{\mathrm{ff\,R}}_{\mathbf{k}}(\varepsilon)$ is the f-electron Green function for quasiparticles given by Eq. (7). The second term in Eq. (16) was not described in Ref. 17, but this term is necessary quantitatively.[24] For example, the exact formula of σ_{xx} derived for $U = 0$ in Sect. 3 is correctly reproduced by Eq. (16) with the second term in the brace when we set $\Sigma^{\mathrm{R}}_{\mathbf{k}}(\varepsilon) = 0$ [see Eq. (55)]. Here, $v_{\mathbf{k}x}(\varepsilon)$ is the total velocity defined as

$$v_{\mathbf{k}x}(\varepsilon) = v^{\mathrm{f}}_{\mathbf{k}x}(\varepsilon) + \left(\frac{V_{\mathbf{k}}}{\varepsilon - \varepsilon_{\mathbf{k}}} \right)^2 v^{\mathrm{c}0}_{\mathbf{k}x} + \frac{\frac{\partial V^2_{\mathbf{k}}}{\partial k_x}}{\varepsilon - \varepsilon_{\mathbf{k}}}, \quad (17)$$

where the velocity of f electrons and conduction electrons are given by

$$v^{\mathrm{f}}_{\mathbf{k}x}(\varepsilon) = v^{\mathrm{f}0}_{\mathbf{k}x} + \frac{\partial \mathrm{Re}\Sigma^{\mathrm{R}}_{\mathbf{k}}(\varepsilon)}{\partial k_x}, \quad (18)$$

$$v^{\rm f0}_{\mathbf{k}x} = \frac{\partial \varepsilon^{\rm f}_{\mathbf{k}}}{\partial k_x}, \tag{19}$$

$$v^{\rm c0}_{\mathbf{k}x} = \frac{\partial \varepsilon_{\mathbf{k}}}{\partial k_x}, \tag{20}$$

respectively. The total current $J_{\mathbf{k}x}(\varepsilon)$ is given by

$$J_{\mathbf{k}x}(\varepsilon) = v_{\mathbf{k}x}(\varepsilon) + \frac{1}{V_0}\sum_{\mathbf{k}'}\int_{-\infty}^{\infty}\frac{d\varepsilon'}{4\pi i}\mathcal{T}_{\mathbf{k}\mathbf{k}'}(\mu,\varepsilon')\left|G^{\rm ff\ R}_{\mathbf{k}'}(\varepsilon')\right|^2 J_{\mathbf{k}'x}(\varepsilon'), \tag{21}$$

where $\mathcal{T}_{\mathbf{k}\mathbf{k}'}(\mu,\varepsilon')$ is the irreducible four-point vertex introduced by Éliashberg.[16] On the basis of the framework of the conserving approximation[21,22] where the general vertex corrections for the total current are considered to be consistent with the self-energy corrections. Yamada and Yosida pointed out that the total current $J_{\mathbf{k}x}(\varepsilon)$ can be obtained as the correct solution of the Bethe-Salpeter equation (21) because of the presence of the Umklapp processes on the periodic crystal lattice.[17] In other words, they stressed that the conductivity due to electron interaction should diverge in the absence of the Umklapp processes as the result of the momentum conservation.

In the case of $\Gamma^* \ll T$, the ε integration in the first-term in Eq. (16), which is denoted by $\sigma^{(1)}_{xx}$, can be performed as

$$\sigma^{(1)}_{xx} \approx \frac{e^2}{V_0}\sum_{\mathbf{k}}\left(-\frac{\partial f(E^{-*}_{\mathbf{k}})}{\partial E^{-*}_{\mathbf{k}}}\right)a^{\rm ff}_{-,\mathbf{k}}v_{\mathbf{k}x}(\mu)\frac{J_{\mathbf{k}x}(\mu)}{-{\rm Im}\Sigma^{\rm R}_{\mathbf{k}}(\mu)}, \tag{22}$$

$$= \frac{e^2}{V_0}\sum_{\mathbf{k}}\delta\left(\mu - E^{-*}_{\mathbf{k}}\right)a^{\rm ff}_{-,\mathbf{k}}v_{\mathbf{k}x}(\mu)\frac{J_{\mathbf{k}x}(\mu)}{-{\rm Im}\Sigma^{\rm R}_{\mathbf{k}}(\mu)}, \tag{23}$$

where the last equation is derived for sufficiently low temperatures. Since the quasiparticle band $E^{-*}_{\mathbf{k}}$ near $\mathbf{k} \approx \mathbf{k}_{\rm F}$ is renormalized by the factor $z_{\mathbf{k}}$, $\delta(\mu - E^{-*}_{\mathbf{k}})$ is enhanced by $z^{-1}_{\mathbf{k}}$. Namely, the mass-renormalization factors $z^{-1}_{\mathbf{k}}$ and $a^{\rm ff}_{-,\mathbf{k}}$ which includes $z_{\mathbf{k}}$ [see Eq. (10)] cancel out each other in Eq. (23). This implies that in σ_{xx}, all renormalizations cancel out and the resistivity is proportional to $-{\rm Im}\Sigma_{\mathbf{k}}(\mu)$. Since within the Fermi liquid theory the imaginary part of the self energy is proportional to T^2 at low temperatures, $-{\rm Im}\Sigma_{\mathbf{k}}(\mu) \propto T^2$, the resistivity $\rho_{xx} = 1/\sigma_{xx}$ shows the T^2 dependence.[17]

As for the normal Hall conductivity, by applying the formalism by Kohno and Yamada[20] to the periodic Anderson model in the case where the single-band treatment is justified with small $\Gamma^*_{\mathbf{k}}$ at sufficiently low temperatures, the Hall conductivity for the lower-hybridized band is given by

$$\sigma_{xy}/H \approx \frac{e^3}{V_0}\sum_{\mathbf{k}}\int_{-\infty}^{\infty}\frac{d\varepsilon}{\pi}\left(-\frac{\partial f(\varepsilon)}{\partial\varepsilon}\right)\left|G^{\rm ff\ R}_{\mathbf{k}}(\varepsilon)\right|^2 {\rm Im}\left[G^{\rm ff\ R}_{\mathbf{k}}(\varepsilon)\right] \times v_{\mathbf{k}x}\left[J_{\mathbf{k}x}\frac{\partial J_{\mathbf{k}y}}{\partial k_y} - J_{\mathbf{k}y}\frac{\partial J_{\mathbf{k}x}}{\partial k_y}\right], \tag{24}$$

where H is a weak magnetic field applied along the z axis. Here, $J_{\mathbf{k}y}$ is the y component of the total current vector $\mathbf{J}_{\mathbf{k}}$, which is given by setting y instead of x in Eq. (21).

In the case of $\Gamma^*_{\mathbf{k}} \ll T$, the ε integration can be performed as

$$\sigma_{xy}/H \approx -\frac{e^3}{V_0}\sum_{\mathbf{k}}\left(-\frac{\partial f(E^{-*}_{\mathbf{k}})}{\partial E^{-*}_{\mathbf{k}}}\right)\left(a^{\rm ff}_{-,\mathbf{k}}\right)^3\frac{1}{2\Gamma^{*2}} \times v_{\mathbf{k}x}\left[J_{\mathbf{k}x}\frac{\partial J_{\mathbf{k}y}}{\partial k_y} - J_{\mathbf{k}y}\frac{\partial J_{\mathbf{k}x}}{\partial k_y}\right], \tag{25}$$

$$= -\frac{e^3}{2V_0}\sum_{\mathbf{k}}\delta\left(\mu - E^{-*}_{\mathbf{k}}\right)\frac{a^{\rm ff}_{-,\mathbf{k}}}{\left[{\rm Im}\Sigma^{\rm R}_{\mathbf{k}}(\mu)\right]^2} \times v_{\mathbf{k}x}\left[J_{\mathbf{k}x}\frac{\partial J_{\mathbf{k}y}}{\partial k_y} - J_{\mathbf{k}y}\frac{\partial J_{\mathbf{k}x}}{\partial k_y}\right], \tag{26}$$

where the last equation is derived for sufficiently low temperatures. Similarly to Eq. (23), enhancement of the density of states of quasiparticles arises from $\delta(\mu - E^{-*}_{\mathbf{k}})$ by factor $z^{-1}_{\mathbf{k}}$, which cancels out by $a^{\rm ff}_{-,\mathbf{k}}$ in Eq. (26). Hence, the mass-enhancement factor does not appear in the expression of the Hall conductivity.

As shown above, the formulas of σ_{xx} and σ_{xy}/H are obtained in the vicinity of the Fermi level located at the lower hybridized band on the basis of the Fermi liquid theory. In both expressions of σ_{xx} and σ_{xy}/H, the renormalization factors of quasiparticles cancel out.

In the next Sect., we will derive the exact formula of σ_{xx} and σ_{xy}/H for $U = 0$ in Eq. (1), which give the general formulas in the two-orbital systems, not restricted to the single band as treated in Eqs. (16) and (24). On the basis of the exactly-derived formulas, we will perform the explicit calculation of σ_{xx} and σ_{xy}/H in the periodic Anderson model with electron correlations to clarify the ground-state properties in Sect.4.

3. Exact formulas of σ_{xx} and σ_{xy} for $U = 0$

In the case of $U = 0$, Eq. (1) is diagonalized as

$$\mathcal{H} = \sum_{\mathbf{k}\sigma}\left[E^-_{\mathbf{k}}\beta^\dagger_{\mathbf{k}\sigma}\beta_{\mathbf{k}\sigma} + E^+_{\mathbf{k}}\gamma^\dagger_{\mathbf{k}\sigma}\gamma_{\mathbf{k}\sigma}\right], \tag{27}$$

where $E^-_{\mathbf{k}}$ is the lower hybridized band and $E^+_{\mathbf{k}}$ is the upper hybridized band, whose explicit form is given by

$$E^\mp_{\mathbf{k}} = \frac{\varepsilon_{\mathbf{k}} + \varepsilon^{\rm f}_{\mathbf{k}}}{2} \mp \frac{\Delta_{\mathbf{k}}}{2}. \tag{28}$$

Here, $\Delta_{\mathbf{k}}$ is defined as

$$\Delta_{\mathbf{k}} = \sqrt{\left(\varepsilon_{\mathbf{k}} - \varepsilon^{\rm f}_{\mathbf{k}}\right)^2 + 4V^2_{\mathbf{k}}}. \tag{29}$$

Equation (27) is obtained by substituting $c^\dagger_{\mathbf{k}\sigma} = u_{\mathbf{k}}\beta^\dagger_{\mathbf{k}\sigma} - w_{\mathbf{k}}\gamma^\dagger_{\mathbf{k}\sigma}$ and $f^\dagger_{\mathbf{k}\sigma} = w_{\mathbf{k}}\beta^\dagger_{\mathbf{k}\sigma} + u_{\mathbf{k}}\gamma^\dagger_{\mathbf{k}\sigma}$ to Eq. (1), where $u_{\mathbf{k}}$ and $w_{\mathbf{k}}$ satisfy

$$u^2_{\mathbf{k}} = a^{\rm cc}_{\mp,\mathbf{k}} = \frac{1}{2}\left(1 \mp \frac{\varepsilon_{\mathbf{k}} - \varepsilon^{\rm f}_{\mathbf{k}}}{\Delta_{\mathbf{k}}}\right), \tag{30}$$

$$w^2_{\mathbf{k}} = a^{\rm ff}_{\mp,\mathbf{k}} = \frac{1}{2}\left(1 \pm \frac{\varepsilon_{\mathbf{k}} - \varepsilon^{\rm f}_{\mathbf{k}}}{\Delta_{\mathbf{k}}}\right), \tag{31}$$

respectively. Here, $a^{\rm cc}_{-,\mathbf{k}}$ ($a^{\rm cc}_{+,\mathbf{k}}$) represents the weight factor of the conduction electrons in the lower (upper) hybridized band and $a^{\rm ff}_{-,\mathbf{k}}$ ($a^{\rm ff}_{+,\mathbf{k}}$) represents the weight factor of the f electrons in the lower (upper) hybridized band. Note that in the case of $U = 0$ in Eq. (1), i.e., $\Sigma^{\rm R}_{\mathbf{k}}(\varepsilon) = 0$, Eqs. (10) and (11) reproduce Eqs. (31) and (30), respectively.

3.1 Derivation of σ_{xx} and σ_{xy}

On the basis of the Kubo formula,[15] the diagonal conductivity is given by

$$\sigma_{xx} = \lim_{\omega\to 0}\frac{\Phi_{xx}(\omega + i\delta) - \Phi_{xx}(0 + i\delta)}{i\omega}. \tag{32}$$

Here, the kernel Φ_{xx} is expressed as

$$\Phi_{xx}(i\omega_m) = -e^2\frac{T}{V_0}\sum_n\sum_{\mathbf{k}\sigma}\mathrm{Tr}\left[\mathcal{G}_{\mathbf{k}\sigma}(i\varepsilon_n)\mathcal{V}_{\mathbf{k}x}\mathcal{G}_{\mathbf{k}\sigma}(i\varepsilon_n+i\omega_m)\mathcal{V}_{\mathbf{k}x}\right] \quad (33)$$

with $\omega_m = 2\pi mT$ and $\varepsilon_n = (2\pi+1)nT$ (m, n are integers). Here, the velocity matrix and the Green-function matrix are given by

$$\mathcal{V}_{\mathbf{k}\eta} = \begin{pmatrix} v^{\mathrm{c0}}_{\mathbf{k}\eta} & \frac{\partial V_{\mathbf{k}}}{\partial k_\eta} \\ \frac{\partial V_{\mathbf{k}}}{\partial k_\eta} & v^{\mathrm{f0}}_{\mathbf{k}\eta} \end{pmatrix}, \quad (34)$$

$$\mathcal{G}_{\mathbf{k}\sigma}(i\varepsilon_n) = \begin{pmatrix} G^{\mathrm{cc}}_{\mathbf{k}\sigma}(i\varepsilon_n) & G^{\mathrm{cf}}_{\mathbf{k}\sigma}(i\varepsilon_n) \\ G^{\mathrm{fc}}_{\mathbf{k}\sigma}(i\varepsilon_n) & G^{\mathrm{ff}}_{\mathbf{k}\sigma}(i\varepsilon_n) \end{pmatrix}, \quad (35)$$

respectively, where

$$G^{\mathrm{ff}}_{\mathbf{k}\sigma}(i\varepsilon_n) = \left[i\varepsilon_n - \varepsilon^{\mathrm{f}}_{\mathbf{k}} - \frac{V_{\mathbf{k}}^2}{i\varepsilon_n-\varepsilon_{\mathbf{k}}}\right]^{-1}, \quad (36)$$

$$G^{\mathrm{cc}}_{\mathbf{k}\sigma}(i\varepsilon_n) = \left[i\varepsilon_n - \varepsilon_{\mathbf{k}} - \frac{V_{\mathbf{k}}^2}{i\varepsilon_n-\varepsilon^{\mathrm{f}}_{\mathbf{k}}}\right]^{-1}, \quad (37)$$

$$G^{\mathrm{cf}}_{\mathbf{k}\sigma}(i\varepsilon_n) = \frac{V_{\mathbf{k}}}{(i\varepsilon_n-\varepsilon^{\mathrm{f}}_{\mathbf{k}})(i\varepsilon_n-\varepsilon_{\mathbf{k}})-V_{\mathbf{k}}^2}, \quad (38)$$

and $G^{\mathrm{fc}}_{\mathbf{k}\sigma}(i\varepsilon_n) = G^{\mathrm{cf}}_{\mathbf{k}\sigma}(i\varepsilon_n)$.

By performing the analytic continuation, the conductivity in the periodic Anderson model for $U = 0$ is derived as

$$\sigma_{xx} = \sigma^{--}_{xx} + \sigma^{++}_{xx} + \sigma^{-+}_{xx} + \sigma^{+-}_{xx}, \quad (39)$$

where

$$\sigma^{--}_{xx} = \frac{e^2}{V_0}\int_{-\infty}^{\infty}\frac{d\varepsilon}{\pi}\left(-\frac{\partial f(\varepsilon)}{\partial\varepsilon}\right)\sum_{\mathbf{k}\sigma}\left(v^{--}_{\mathbf{k}x}\right)^2\left\{\mathrm{Im}G^{-\mathrm{R}}_{\mathbf{k}\sigma}(\varepsilon)\right\}^2, \quad (40)$$

$$\sigma^{++}_{xx} = \frac{e^2}{V_0}\int_{-\infty}^{\infty}\frac{d\varepsilon}{\pi}\left(-\frac{\partial f(\varepsilon)}{\partial\varepsilon}\right)\sum_{\mathbf{k}\sigma}\left(v^{++}_{\mathbf{k}x}\right)^2\left\{\mathrm{Im}G^{+\mathrm{R}}_{\mathbf{k}\sigma}(\varepsilon)\right\}^2, \quad (41)$$

$$\sigma^{-+}_{xx}+\sigma^{+-}_{xx} = \frac{e^2}{V_0}\int_{-\infty}^{\infty}\frac{d\varepsilon}{\pi}\left(-\frac{\partial f(\varepsilon)}{\partial\varepsilon}\right)\sum_{\mathbf{k}\sigma}v^{-+}_{\mathbf{k}x}v^{+-}_{\mathbf{k}x} \times\mathrm{Re}\left[G^{-\mathrm{R}}_{\mathbf{k}\sigma}(\varepsilon)G^{+\mathrm{A}}_{\mathbf{k}\sigma}(\varepsilon)-G^{-\mathrm{R}}_{\mathbf{k}\sigma}(\varepsilon)G^{+\mathrm{R}}_{\mathbf{k}\sigma}(\varepsilon)\right]. \quad (42)$$

Here, V_0 is a volume of the system. The velocity of the hybridized band $v^{\alpha\alpha}_{\mathbf{k}\eta} \equiv \partial E^{(\alpha)}_{\mathbf{k}}/\partial k_\eta$ ($\eta = x, y, z$) is given by

$$v^{\alpha\alpha}_{\mathbf{k}\eta} = a^{\mathrm{cc}}_{\alpha,\mathbf{k}}v^{\mathrm{c0}}_{\mathbf{k}\eta} + a^{\mathrm{ff}}_{\alpha,\mathbf{k}}v^{\mathrm{f0}}_{\mathbf{k}\eta} + a^{\mathrm{cf}}_{\alpha,\mathbf{k}}\frac{\partial V_{\mathbf{k}}}{\partial k_\eta} + a^{\mathrm{fc}}_{\alpha,\mathbf{k}}\frac{\partial V_{\mathbf{k}}}{\partial k_\eta}, \quad (43)$$

where $a^{\mathrm{cf}}_{\mp,\mathbf{k}}$ and $a^{\mathrm{fc}}_{\mp,\mathbf{k}}$ are defined as

$$a^{\mathrm{cf}}_{-,\mathbf{k}} = -\frac{V_{\mathbf{k}}}{\Delta_{\mathbf{k}}}, \quad a^{\mathrm{cf}}_{+,\mathbf{k}} = \frac{V_{\mathbf{k}}}{\Delta_{\mathbf{k}}}, \quad (44)$$

$$a^{\mathrm{fc}}_{-,\mathbf{k}} = -\frac{V_{\mathbf{k}}}{\Delta_{\mathbf{k}}}, \quad a^{\mathrm{fc}}_{+,\mathbf{k}} = \frac{V_{\mathbf{k}}}{\Delta_{\mathbf{k}}}, \quad (45)$$

respectively, which satisfies $a^{\mathrm{ff}}_{\mp,\mathbf{k}} + a^{\mathrm{cc}}_{\mp,\mathbf{k}} = 1$ and $a^{\mathrm{ff}}_{\alpha,\mathbf{k}}a^{\mathrm{cc}}_{\alpha,\mathbf{k}} = a^{\mathrm{cf}}_{\alpha,\mathbf{k}}a^{\mathrm{fc}}_{\alpha,\mathbf{k}}$. In Eq. (42), the off-diagonal velocity is defined as

$$v^{\alpha\overline{\alpha}}_{\mathbf{k}\eta} = \sqrt{a^{\mathrm{cc}}_{\alpha,\mathbf{k}}a^{\mathrm{cc}}_{\overline{\alpha},\mathbf{k}}}\,v^{\mathrm{c0}}_{\mathbf{k}\eta} + \sqrt{a^{\mathrm{ff}}_{\alpha,\mathbf{k}}a^{\mathrm{ff}}_{\overline{\alpha},\mathbf{k}}}\,v^{\mathrm{f0}}_{\mathbf{k}\eta} + \sqrt{a^{\mathrm{cc}}_{\alpha,\mathbf{k}}a^{\mathrm{ff}}_{\overline{\alpha},\mathbf{k}}}\frac{\partial V_{\mathbf{k}}}{\partial k_\eta} + \sqrt{a^{\mathrm{ff}}_{\alpha,\mathbf{k}}a^{\mathrm{cc}}_{\overline{\alpha},\mathbf{k}}}\frac{\partial V_{\mathbf{k}}}{\partial k_\eta} \quad (46)$$

for $\overline{\alpha} = -\alpha$.

The retarded Green function $G^{\alpha\mathrm{R}}_{\mathbf{k}\sigma}(\varepsilon)$ is given by

$$G^{\alpha\mathrm{R}}_{\mathbf{k}\sigma}(\varepsilon) = \frac{1}{\varepsilon - E^{(\alpha)}_{\mathbf{k}} + i\Gamma^{(\alpha)}_{\mathbf{k}}}. \quad (47)$$

The advanced Green function $G^{\alpha\mathrm{A}}_{\mathbf{k}\sigma}(\varepsilon)$ is obtained by the relation of $G^{\alpha\mathrm{A}}_{\mathbf{k}\sigma}(\varepsilon) = \left[G^{\alpha\mathrm{R}}_{\mathbf{k}\sigma}(\varepsilon)\right]^*$. Here, we introduce the imaginary part of the self energy $\Gamma^{(\alpha)}_{\mathbf{k}}$ in Eq. (47). This term can arise from the impurity scattering even in the $U = 0$ periodic Anderson model. We discuss the general expression of σ_{xx} and σ_{xy}/H with the finite damping rate.

On the basis of the formalism in Refs. 18, 19, the Hall conductivity in the periodic Anderson model for $U = 0$ is derived. Hereafter, we show the result for $V_{\mathbf{k}} = V$ in Eq. (1).

The Hall conductivity is given by

$$\sigma_{xy} = \lim_{\omega\to0}\lim_{\mathbf{q}\to\mathbf{0}}\frac{\Phi_{xy}(\mathbf{q},\omega+i\delta)-\Phi_{xy}(\mathbf{q},i\delta)}{i\omega}, \quad (48)$$

where the kernel $\Phi_{xy}(\mathbf{q}, i\omega_m)$ is given by

$$\Phi_{xy}(\mathbf{q},i\omega_m) = (q_xA_{\mathbf{q}y}-q_yA_{\mathbf{q}x})e^3\frac{T}{2V_0}\sum_n\sum_{\mathbf{k}\sigma}\mathrm{Tr}\Big[\mathcal{V}_{\mathbf{k}x}\left(\frac{\partial}{\partial k_x}\mathcal{G}_{\mathbf{k}\sigma}(i\varepsilon_n)\right)\left(\frac{\partial\mathcal{V}_{\mathbf{k}y}}{\partial k_y}\right)\mathcal{G}_{\mathbf{k}\sigma}(i\varepsilon_n+i\omega_m) -\mathcal{V}_{\mathbf{k}x}\mathcal{G}_{\mathbf{k}\sigma}(i\varepsilon_n)\left(\frac{\partial\mathcal{V}_{\mathbf{k}y}}{\partial k_y}\right)\frac{\partial}{\partial k_x}\mathcal{G}_{\mathbf{k}\sigma}(i\varepsilon_n+i\omega_m) +\left(v_{\mathbf{k}x}\leftrightarrow v_{\mathbf{k}y}\right)\Big]. \quad (49)$$

Here $A_{\mathbf{q}\eta}$ is the η component of the vector potential by which the magnetic field along the z axis is expressed as $H = i\lim_{\mathbf{q}\to0}(q_xA_{\mathbf{q}y} - q_yA_{\mathbf{q}x})$. By performing the analytic continuation, the Hall conductivity is obtained as follows:

$$\sigma_{xy} = \sum_{\alpha=\mp}\sigma^{\alpha\alpha}_{xy} + \sum_{\alpha=\mp}\sigma^{\alpha\overline{\alpha}}_{xy} + \sigma^{\mathrm{extra}}_{xy}, \quad (50)$$

where

$$\sigma^{\alpha\alpha}_{xy} = H\frac{e^3}{2V_0}\sum_{\mathbf{k}\sigma}\int_{-\infty}^{\infty}\frac{d\varepsilon}{\pi}\left(-\frac{\partial f(\varepsilon)}{\partial\varepsilon}\right)\left|G^{\alpha\mathrm{R}}_{\mathbf{k}\sigma}(\varepsilon)\right|^2\mathrm{Im}\left[G^{\alpha\mathrm{R}}_{\mathbf{k}\sigma}(\varepsilon)\right] \times v^{\alpha\alpha}_{\mathbf{k}x}\left(v^{\alpha\alpha}_{\mathbf{k}x}\frac{\partial v^{\alpha\alpha}_{\mathbf{k}y}}{\partial k_y}-v^{\alpha\alpha}_{\mathbf{k}y}\frac{\partial v^{\alpha\alpha}_{\mathbf{k}x}}{\partial k_y}\right), \quad (51)$$

$$\sigma^{\alpha\overline{\alpha}}_{xy} = H\frac{e^3}{2V_0}\sum_{\mathbf{k}\sigma}\int_{-\infty}^{\infty}\frac{d\varepsilon}{\pi}\left(-\frac{\partial f(\varepsilon)}{\partial\varepsilon}\right)\mathrm{Im}\left[\left\{G^{\alpha\mathrm{R}}_{\mathbf{k}\sigma}(\varepsilon)\right\}^2G^{\overline{\alpha}\mathrm{A}}_{\mathbf{k}\sigma}(\varepsilon)\right] \times v^{\alpha\alpha}_{\mathbf{k}x}\left(v^{\alpha\overline{\alpha}}_{\mathbf{k}x}\frac{\partial v^{\overline{\alpha}\alpha}_{\mathbf{k}y}}{\partial k_y}-v^{\alpha\overline{\alpha}}_{\mathbf{k}y}\frac{\partial v^{\overline{\alpha}\alpha}_{\mathbf{k}x}}{\partial k_y}\right) - H\frac{e^3}{2V_0}\sum_{\mathbf{k}\sigma}\int_{-\infty}^{\infty}\frac{d\varepsilon}{\pi}f(\varepsilon)\mathrm{Im}\Big[-2\left\{G^{\alpha\mathrm{R}}_{\mathbf{k}\sigma}(\varepsilon)\right\}^3G^{\overline{\alpha}\mathrm{R}}_{\mathbf{k}\sigma}(\varepsilon) +\left\{G^{\alpha\mathrm{R}}_{\mathbf{k}\sigma}(\varepsilon)\right\}^2\left\{G^{\overline{\alpha}\mathrm{R}}_{\mathbf{k}\sigma}(\varepsilon)\right\}^2\Big]v^{\alpha\alpha}_{\mathbf{k}x}\left(v^{\alpha\overline{\alpha}}_{\mathbf{k}x}\frac{\partial v^{\overline{\alpha}\alpha}_{\mathbf{k}y}}{\partial k_y}-v^{\alpha\overline{\alpha}}_{\mathbf{k}y}\frac{\partial v^{\overline{\alpha}\alpha}_{\mathbf{k}x}}{\partial k_y}\right), \quad (52)$$

$$\sigma^{\mathrm{extra}}_{xy} = H\frac{e^3}{2V_0}\sum_{\mathbf{k}\sigma}\int_{-\infty}^{\infty}\frac{d\varepsilon}{\pi}\left(-\frac{\partial f(\varepsilon)}{\partial\varepsilon}\right)\mathrm{Im}\left[G^{-\mathrm{R}}_{\mathbf{k}\sigma}(\varepsilon)G^{+\mathrm{A}}_{\mathbf{k}\sigma}(\varepsilon)\right]Q_{\mathbf{k}xy} - H\frac{e^3}{2V_0}\sum_{\mathbf{k}\sigma}\int_{-\infty}^{\infty}\frac{d\varepsilon}{\pi}f(\varepsilon)\mathrm{Im}\Big[-\left\{G^{-\mathrm{R}}_{\mathbf{k}\sigma}(\varepsilon)\right\}^2G^{+\mathrm{R}}_{\mathbf{k}\sigma}(\varepsilon)$$

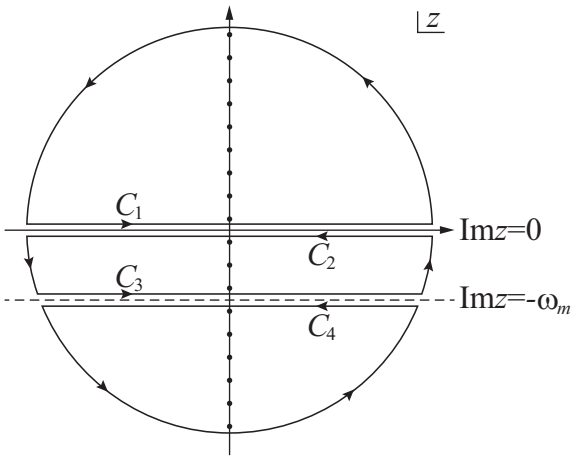

Fig. 1. Contours of integration in the complex-z plane. The dots on the imaginary axis represent the Fermionic thermal frequencies $i\varepsilon_n = i(2n+1)\pi T$ with n being integers.

$$+G^{-\mathrm{R}}_{\mathbf{k}\sigma}(\varepsilon)\left\{G^{+\mathrm{R}}_{\mathbf{k}\sigma}(\varepsilon)\right\}^2\Big] Q_{\mathbf{k}xy}. \tag{53}$$

Here, $\overline{\alpha} = -\alpha$ and $Q_{\mathbf{k}xy}$ is defined by

$$\begin{aligned} Q_{\mathbf{k}xy} &= -2\frac{v^{\mathrm{c0}}_{\mathbf{k}x} - v^{\mathrm{f0}}_{\mathbf{k}x}}{\Delta_{\mathbf{k}}}\frac{V^2}{\Delta^2_{\mathbf{k}}} \\ &\times \left(v^{\mathrm{c0}}_{\mathbf{k}x}\frac{\partial v^{\mathrm{c0}}_{\mathbf{k}y}}{\partial k_y} - v^{\mathrm{c0}}_{\mathbf{k}y}\frac{\partial v^{\mathrm{c0}}_{\mathbf{k}x}}{\partial k_y} + v^{\mathrm{f0}}_{\mathbf{k}x}\frac{\partial v^{\mathrm{f0}}_{\mathbf{k}y}}{\partial k_y} - v^{\mathrm{f0}}_{\mathbf{k}y}\frac{\partial v^{\mathrm{f0}}_{\mathbf{k}x}}{\partial k_y}\right) \end{aligned} \tag{54}$$

In deriving Eq. (39) and Eq. (50), the analytic continuation is performed as shown in Fig. 1.[16,18,20,25–28] Here, C_1 (C_2) is the contour from $-\infty$ to ∞ (from ∞ to $-\infty$) at just above (below) Imz = 0 and C_3 (C_4) is the contour from $-\infty$ to ∞ (from ∞ to $-\infty$) at just above (below) Im$z = -\omega_m$. In Eq. (39) and Eq. (50), the term including $f'(\varepsilon)$ term arises from the C_2+C_3 contours, which makes the main contribution come from the vicinity of the Femi level. On the other hand, in Eq. (50), the term including $f(\varepsilon)$ term arises from the contribution from the $C_1 + C_4$ contours.

It is noted that even when the hybridization has the momentum dependence, $V_{\mathbf{k}}$, Eqs. (51) and (52) hold with the velocities defined in Eqs. (43) and (46). Equaions (39) and Eq. (50) are the general expressions for σ_{xx} and σ_{xy}/H, respectively, in the systems with the single-band as well as the two-bands at the Fermi level, which are constituted of two orbitals.

To clarify the fundamental properties of the conductivity and Hall coefficient in the periodic Anderson model, hereafter we discuss the case of the flat dispersion of the f band, $\varepsilon^{\mathrm{f}}_{\mathbf{k}} = \varepsilon_{\mathrm{f}}$ in Eq. (1) as the simplest typical case of the heavy-electron systems.

An important remark is that in Eqs. (39) and (50) the velocities of the hybridized bands $v^{\alpha\alpha}_{\mathbf{k}\eta}$ appear, which give rise to the velocity of the "large" Fermi surface which contains contributions from both f and conduction electrons, but not of the "small" Fermi surface for the conduction band.

3.2 The limit of small damping rate at low temperatures

When the total filling is less than the half-filling, i.e., $\overline{n} < 2$ and the Fermi level is located at the lower hybridized band, $\sigma_{xx} = \sigma^{--}_{xx}$ holds in Eq. (39) at low temperatures for the small $\Gamma^-_{\mathbf{k}}$ to satisfy $\omega\tau^-_{\mathbf{k}} \gg 1$, where the relaxation time $\tau^-_{\mathbf{k}}$ is defined as $\tau^-_{\mathbf{k}} \equiv \frac{1}{2\Gamma^-_{\mathbf{k}}}$.

In this case, from Eq. (40), we have

$$\begin{aligned} \sigma_{xx} \approx \sigma^{--}_{xx} &= \frac{e^2}{V_0}\sum_{\mathbf{k}\sigma}\left(-\frac{\partial f(E^-_{\mathbf{k}})}{\partial E^-_{\mathbf{k}}}\right)\left(v^{\mathrm{c0}}_{\mathbf{k}x}\right)^2\left(a^{\mathrm{cc}}_{-,\mathbf{k}}\right)^2 \\ &\times\int_{-\infty}^{\infty}\frac{d\varepsilon}{\pi}\left[\frac{\Gamma^-_{\mathbf{k}}}{(\varepsilon - E^-_{\mathbf{k}})^2 + \Gamma^{-2}_{\mathbf{k}}}\right]^2, \\ &= \frac{e^2}{V_0}\sum_{\mathbf{k}\sigma}\left(-\frac{\partial f(E^-_{\mathbf{k}})}{\partial E^-_{\mathbf{k}}}\right)\left(v^{\mathrm{c0}}_{\mathbf{k}x}\right)^2\left(a^{\mathrm{cc}}_{-,\mathbf{k}}\right)^2\frac{1}{2\Gamma^-_{\mathbf{k}}}, \\ &= \frac{e^2}{V_0}\sum_{\mathbf{k}\sigma}\left(-\frac{\partial f(E^-_{\mathbf{k}})}{\partial E^-_{\mathbf{k}}}\right)\left(v^{\mathrm{c0}}_{\mathbf{k}x}\right)^2\left(a^{\mathrm{cc}}_{-,\mathbf{k}}\right)^2\tau^-_{\mathbf{k}}. \end{aligned} \tag{55}$$

Note that Eq. (16) in the limit of $U = 0$ reproduces the expression of Eq. (55). Since $-\frac{\partial f(E^-_{\mathbf{k}})}{\partial E^-_{\mathbf{k}}} = \delta(\mu - E^-_{\mathbf{k}})$ holds at $T = 0$, we have

$$\sigma_{xx} = \frac{e^2}{V_0}\sum_{\mathbf{k}\sigma}\delta(\mu - E^-_{\mathbf{k}})\left(v^{\mathrm{c0}}_{\mathbf{k}x}\right)^2\left(a^{\mathrm{cc}}_{-,\mathbf{k}}\right)^2\tau^-_{\mathbf{k}}, \tag{56}$$

in the ground state.

As for the Hall conductivity, in the small $\Gamma^-_{\mathbf{k}}$ limit at low temperatures, the contribution from the lower hybridized band σ^{--}_{xy} in Eq. (51) is only the relevant term for σ_{xy}. Then we have

$$\begin{aligned} \sigma_{xy} &\approx H\frac{e^3}{2V_0}\sum_{\mathbf{k}\sigma}\left(-\frac{\partial f(E^-_{\mathbf{k}})}{\partial E^-_{\mathbf{k}}}\right)\left(v^{\mathrm{c0}}_{\mathbf{k}x}\right)^2\left(\frac{\partial v^{\mathrm{c0}}_{\mathbf{k}y}}{\partial k_y}\right)\left(a^{\mathrm{cc}}_{-,\mathbf{k}}\right)^3 \\ &\times\int_{-\infty}^{\infty}\frac{d\varepsilon}{\pi}\left|G^{-\mathrm{R}}_{\mathbf{k}\sigma}(\varepsilon)\right|^2\mathrm{Im}G^{-\mathrm{R}}_{\mathbf{k}\sigma}(\varepsilon), \\ &= -H\frac{e^3}{2V_0}\sum_{\mathbf{k}\sigma}\left(-\frac{\partial f(E^-_{\mathbf{k}})}{\partial E^-_{\mathbf{k}}}\right)\left(v^{\mathrm{c0}}_{\mathbf{k}x}\right)^2\left(\frac{\partial v^{\mathrm{c0}}_{\mathbf{k}y}}{\partial k_y}\right)\left(a^{\mathrm{cc}}_{-,\mathbf{k}}\right)^3 2\tau^{-2}_{\mathbf{k}}, \end{aligned} \tag{57}$$

Note that Eq. (24) in the limit of $U = 0$ reproduces the expression of Eq. (57). Since $-\frac{\partial f(E^-_{\mathbf{k}})}{\partial E^-_{\mathbf{k}}} = \delta(\mu - E^-_{\mathbf{k}})$ holds at $T = 0$, we have

$$\sigma_{xy} = -H\frac{e^3}{2V_0}\sum_{\mathbf{k}\sigma}\delta(\mu - E^-_{\mathbf{k}})\left(v^{\mathrm{c0}}_{\mathbf{k}x}\right)^2\left(\frac{\partial v^{\mathrm{c0}}_{\mathbf{k}y}}{\partial k_y}\right)\left(a^{\mathrm{cc}}_{-,\mathbf{k}}\right)^3 2\tau^{-2}_{\mathbf{k}}, \tag{58}$$

in the ground state.

3.3 Isotropic free-electron system

To analyze σ_{xx} and σ_{xy} explicitly, we consider the isotropic free electron system. Namely, the conduction electrons have the free dispersion as $\varepsilon_{\mathbf{k}} = \frac{k^2}{2m_c}$ in the periodic Anderson model in three spatial dimension. Here we assume $\tau = \tau^-_{\mathbf{k}}$ ($\Gamma = \Gamma^-_{\mathbf{k}}$) for simplicity of analysis. Equation (56) can be calculated as

$$\sigma_{xx} = \frac{2e^2\tau}{(2\pi)^3}\int_{S(\mu)}dS\,\frac{\left(v^{\mathrm{c0}}_{\mathbf{k}x}\right)^2\left(a^{\mathrm{cc}}_{-,\mathbf{k}}\right)^2}{\left|\nabla E^-_{\mathbf{k}}\right|}, \tag{59}$$

where the integral is taken as the surface integral over the constant-energy-surface $S(\mu)$ where $\mu = E^-_{\mathbf{k}}$ is satisfied in the $\mathbf{k}$ space.[29] Since we have $\left|\nabla E^-_{\mathbf{k}}\right| = a^{\mathrm{cc}}_{-,\mathbf{k}}v^{\mathrm{c0}}_k$ with $v^{\mathrm{c0}}_k \equiv \sqrt{(v^{\mathrm{c0}}_{\mathbf{k}x})^2 + (v^{\mathrm{c0}}_{\mathbf{k}y})^2 + (v^{\mathrm{c0}}_{\mathbf{k}z})^2}$ and $\int_{S(\mu)}dS = 4\pi k^2_{\mathrm{F}}$ with k_{F} being the Fermi wave number in the isotropic free-electron system,

Eq. (59) leads to

$$\sigma_{xx} = \frac{2e^2\tau}{(2\pi)^3}4\pi k_{\rm F}^2\frac{\left(v^{\rm c0}_{k_{\rm F}x}\right)^2 a^{\rm cc}_{-,k_{\rm F}}}{v^{\rm c0}_{k_{\rm F}}}, \quad (60)$$

$$= \frac{\bar{n}e^2\tau}{m_{\rm c}}a^{\rm cc}_{-,k_{\rm F}}, \quad (61)$$

where $v^{\rm c0}_{k_{\rm F}} = k_{\rm F}/m_{\rm c}$, $v^{\rm c0}_{k_{\rm F}x} = k_{{\rm F}x}/m_{\rm c}$, and $k^2_{{\rm F}x} = k^2_{\rm F}/3$ are used. Here, $\bar{n}$ is the total filling, which is defined by the total electron number $N_{\rm e}$ per the volume of the system:

$$\bar{n} = \frac{N_{\rm e}}{V_0} = 2\frac{4\pi}{(2\pi)^3}\int_0^{k_{\rm F}} dkk^2 = \frac{k_{\rm F}^3}{3\pi^2}. \quad (62)$$

Note that the factor $\tau a^{\rm cc}_{-,k_{\rm F}}$ appears in Eq. (61), which implies that the ratio of the amplitude of conduction electrons to the damping rate determines the nature of σ_{xx}.

As for the Hall conductivity, Eq. (58) can be calculated as

$$\sigma_{xy} = -H\frac{2e^3\tau^2}{(2\pi)^3 m_{\rm c}}\int_{S(\mu)} dS\frac{\left(v^{\rm c0}_{{\bf k}x}\right)^2\left(a^{\rm cc}_{-,{\bf k}}\right)^3}{\left|\nabla E^-_{\bf k}\right|}, \quad (63)$$

$$= -H\frac{2e^3\tau^2}{(2\pi)^3 m_{\rm c}}4\pi k_{\rm F}^2\frac{\left(v^{\rm c0}_{k_{\rm F}x}\right)^2\left(a^{\rm cc}_{-,k_{\rm F}}\right)^2}{v_{k_{\rm F}}}, \quad (64)$$

$$= -\omega_{\rm c}\tau\sigma_{xx}a^{\rm cc}_{-,k_{\rm F}}, \quad (65)$$

where ω_c is the cyclotron frequency defined as $\omega_{\rm c} \equiv \frac{eH}{m_{\rm c}}$. Note that in Eq. (64) the factor $\left(\tau a^{\rm cc}_{-,k_{\rm F}}\right)^2$ appears, which implies that the square of the ratio of the amplitude of conduction electrons to the damping rate determines the nature of σ_{xy}.

By using Eqs. (61) and (65), the Hall coefficient $R_{\rm H}$ under a weak magnetic field H applied along the z axis is obtained as

$$R_{\rm H} = \frac{\sigma_{xy}/H}{\sigma_{xx}^2}, \quad (66)$$

$$= -\frac{\omega_{\rm c}\tau a^{\rm cc}_{-,k_{\rm F}}}{H\sigma_{xx}}, \quad (67)$$

$$= -\frac{1}{\bar{n}e}. \quad (68)$$

Note here that although both σ_{xx} and σ_{xy} include the ratio of the weight factor $a^{\rm cc}_{-,k_{\rm F}}$ to the damping rate as Eqs. (61) and (65), the factors $\tau a^{\rm cc}_{-,k_{\rm F}}$ in the Hall coefficient are cancelled so that the resultant $R_{\rm H}$ is expressed by the total electron filling $\bar{n}$. This implies that $R_{\rm H}$ is only determined by the total filling irrespective of the weight of conduction electrons component at the Fermi level. Namely, Eq. (68) reproduces the well-known result in the single-orbital system.

Here, two remarks should be made. First, Eq. (68) shows the negative sign and that the magnitude is expressed as inverse of the total filling. We note that Eq. (68) is obtained in the free-electron system with the spherical Fermi surface. In general, $R_{\rm H}$ depends on the shape of the Fermi surface, more precisely, the curvature of the Fermi surface. Hence, sign of $R_{\rm H}$ and the magnitude itself depend on the shape of the Fermi surface even in the small-$\Gamma^-_{\bf k}$ limit at $T = 0$. This point will be discussed in detail in Sect. 4.2.5.

Second, we note that Eq. (68) is obtained in the small-$\Gamma^-_{\bf k}$ limit. If the damping rate $\Gamma^-_{\bf k}$ is not small, it is not guaranteed that $R_{\rm H}$ shows a constant behavior as Eq. (68) when $\omega_{\rm c}$ is varied even at $T = 0$, as will be discussed in Sect. 4.2.6.

4. Ground-state properties of σ_{xx}, σ_{xy}/H, and $R_{\rm H}$ on the square lattice

In Sect. 3, we derived exactly the general expressions of diagonal and Hall conductivities in hybridized two-orbital systems with arbitrary band dispersions for non-interacting case. In this Sect. we study the ground-state properties of the diagonal conductivity and normal Hall effect in the periodic Anderson model with onsite Coulomb repulsion between f electrons. By employing the Fermi liquid theory discussed in Sect. 2, we will discuss that the diagonal and Hall conductivities can be calculated by using the formulas derived in Sect. 3. However, we make an approximation in which the Fermi liquid correction for the current given by Eq. (21) is neglected. Nevertheless, this approximation is considered to be valid for the present purpose that we discuss a qualitative aspect of the diagonal and Hall conductivities. To clarify the general properties realized in Ce- and Yb-based heavy-electron systems, we concentrate on the Fermi-liquid ground state taking into account the effect of weak impurity scatterings.

The imaginary part of the f-electron self energy around the Fermi level is expressed as

$${\rm Im}\Sigma^{\rm R}_{\bf k}(\varepsilon) = {\rm Im}\Sigma^{U\ {\rm R}}_{\bf k}(\varepsilon) + {\rm Im}\Sigma^{\rm imp\ R}, \quad (69)$$

where ${\rm Im}\Sigma^{U\ {\rm R}}_{\bf k}(\varepsilon)$ is arising from the onsite Coulomb repulsion in Eq. (1) and ${\rm Im}\Sigma^{\rm imp\ R}$ is from the impurity scattering. In the Fermi-liquid regime, ${\rm Im}\Sigma^{U\ {\rm R}}_{\bf k}(\varepsilon)$ has the following form at zero temperature:

$${\rm Im}\Sigma^{U\ {\rm R}}_{\bf k}(\varepsilon) = -C_U(\varepsilon-\mu)^2, \quad (70)$$

where $C_U > 0$ is a constant of the order of the inverse of the effective Fermi energy.[17,30] When f electrons are scattered weakly by a small amount of local impurities, ${\rm Im}\Sigma^{\rm imp\ R}$ is calculated within the Born approximation[30,31] as

$${\rm Im}\Sigma^{\rm imp\ R} \approx -\pi n_{\rm imp}u^2\langle a^{\rm ff}_{-,{\bf k}_{\rm F}}\rangle_{\rm av}N^*(\mu), \quad (71)$$

where $n_{\rm imp}$ is the impurity concentration and u is the impurity potential. Here, $N^*(\mu)$ is the density of states of the quasiparticles at the Fermi level defined by $N^*(\varepsilon) \equiv \sum_{\bf k}\delta(\varepsilon - E^-_{\bf k})/N$ with N being the number of lattice sites and $\langle a^{\rm ff}_{-,{\bf k}_{\rm F}}\rangle_{\rm av}$ is averaged value of the f-electron weight factor defined in Eq. (10) over the Fermi level. Although $N^*(\mu)$ is enhanced by the renormalization factor $z^{-1}_{{\bf k}_{\rm F}}$, the enhancement is canceled by the factor $\langle a^{\rm ff}_{-,{\bf k}}\rangle_{\rm av}$ [see Eq. (10)]. Hence, $\langle a^{\rm ff}_{-,{\bf k}_{\rm F}}\rangle_{\rm av}N^*(\mu)$ is the quantity in the order of $(\pi V^2 N_{\rm cF})^{-1}$, where $N_{\rm cF}$ is the density of states of conduction electrons at the Fermi level.

As described in the formalism in Sect. 2, the diagonal conductivity in Eq. (16) and Hall conductivity in Eq. (24) are claculated by using the Green function for quasiparticles. Here we consider the ${\rm Im}\Sigma^{\rm R}_{\bf k}(\mu)$ in the form of Eq. (69) as the self energy. Since the impurity concentration $n_{\rm imp}$ and the strength of the impurity potential u are parameters to be given and the extra factor $\langle a^{\rm ff}_{-,{\bf k}_{\rm F}}\rangle_{\rm av}N^*(\mu)$ in Eq. (71) can be expressed essentially by bare quantities not including renormalization factor and has only weak dependence in $\varepsilon_{\rm f}$, we treat them as variable input parameters. Namely, we calculate σ_{xx} and σ_{xy}/H by inputting

$$\Gamma \equiv -{\rm Im}\Sigma^{\rm R}_{\bf k}(\mu) = -{\rm Im}\Sigma^{\rm imp\ R} \quad (72)$$

into the quasiparticle Green function. As the simplest framework to perform such a calculation, we employ the slave-boson mean field theory[32] since it has been established to describe the fixed point of the Fermi-liquid ground state in the periodic Anderson model correctly.

4.1 Slave-boson mean field theory

By applying the slave-boson mean field theory[32] to Eq. (1), the effective Hamiltonian is obtained as

$$\begin{aligned}\tilde{\mathcal{H}} &= \sum_{\mathbf{k}\sigma}\varepsilon_{\mathbf{k}}c^{\dagger}_{\mathbf{k}\sigma}c_{\mathbf{k}\sigma}+\sum_{i\sigma}\varepsilon_{\mathrm{f}}f^{\dagger}_{i\sigma}f_{i\sigma}\\ &+ V\sum_{i\sigma}\left(z_{i\sigma}f^{\dagger}_{i\sigma}c_{i\sigma}+c^{\dagger}_{i\sigma}f_{i\sigma}z^{\dagger}_{i\sigma}\right)+U\sum_{i}d^{\dagger}_{i}d_{i}\\ &+ \sum_{i}\lambda^{(1)}_{i}\left(e^{\dagger}_{i}e_{i}+p^{\uparrow}_{i\sigma}p_{i\uparrow}+p^{\dagger}_{i\downarrow}p_{i\downarrow}+d^{\dagger}_{i}d_{i}-1\right)\\ &+ \sum_{i\sigma}\lambda^{(2)}_{i\sigma}\left(f^{\dagger}_{i\sigma}f_{i\sigma}-p^{\dagger}_{i\sigma}p_{i\sigma}-d^{\dagger}_{i}d_{i}\right). \qquad (73)\end{aligned}$$

Here, $e^{\dagger}_{i}$ (e_i) and $d^{\dagger}_{i}$ (d_i) are bose creation (annihilation) operators for the empty and doubly-occupied state, respectively and $p^{\dagger}_{i\sigma}$ ($p_{i\sigma}$) for the singly-occupied state on the i-th site. The renormalization factor is defined as

$$\begin{aligned}z_{i\sigma} &\equiv \left(1-d^{\dagger}_{i}d_{i}-p^{\dagger}_{i\sigma}p_{i\sigma}\right)^{-1/2}\left(e^{\dagger}_{i}p_{i\sigma}+p^{\dagger}_{i-\sigma}d_{i}\right)\\ &\times\left(1-e^{\dagger}_{i}e_{i}-p^{\dagger}_{i-\sigma}p_{i-\sigma}\right)^{-1/2}. \qquad (74)\end{aligned}$$

The last two terms with the Lagrange multipliers $\lambda^{(1)}_{i}$ and $\lambda^{(2)}_{i}$ in Eq. (73) are introduced to require the constraint for the completeness condition.

Here, we consider the case where f electrons are subject to the impurity scattering in the form of Eq. (72) as an input parameter.

By approximating the mean fields as uniform ones, $e=\langle e_i\rangle$, $p_\sigma=\langle p_{i\sigma}\rangle$, $d=\langle d_i\rangle$, and the Lagrange multipliers, $\lambda^{(1)}=\lambda^{(1)}_{i}$ and $\lambda^{(2)}=\lambda^{(2)}_{i}$, with $z_\sigma=\langle z_{i\sigma}\rangle$, the set of mean-field equations is obtained by $\partial\langle\tilde{\mathcal{H}}\rangle/\partial\lambda^{(1)}=0$, $\partial\langle\tilde{\mathcal{H}}\rangle/\partial\lambda^{(2)}=0$, $\partial\langle\tilde{\mathcal{H}}\rangle/\partial p_\uparrow=0$, $\partial\langle\tilde{\mathcal{H}}\rangle/\partial p_\downarrow=0$, $\partial\langle\tilde{\mathcal{H}}\rangle/\partial d=0$, and $\partial\langle\tilde{\mathcal{H}}\rangle/\partial e=0$:

$$e^2+p^2_{\uparrow}+p^2_{\downarrow}+d^2 = 1, \qquad (75)$$

$$\frac{1}{N}\sum_{\mathbf{k}\sigma}\langle f^{\dagger}_{\mathbf{k}\sigma}f_{\mathbf{k}\sigma}\rangle = p^2_{\uparrow}+p^2_{\downarrow}, \qquad (76)$$

$$\begin{aligned}&\frac{V}{N}\sum_{\mathbf{k}\sigma}\left(\frac{\partial z_\sigma}{\partial p_\uparrow}\right)\left(\langle f^{\dagger}_{\mathbf{k}\sigma}c_{\mathbf{k}\sigma}\rangle+\mathrm{h.c.}\right)\\ &+2\sum_{\mathbf{k}\sigma}z_\sigma\left(\frac{\partial z_\sigma}{\partial p_\uparrow}\right)\varepsilon_{\mathrm{f}}\langle f^{\dagger}_{\mathbf{k}\sigma}f_{\mathbf{k}\sigma}\rangle = -2\left(\lambda^{(1)}-\lambda^{(2)}\right)p_\uparrow, \qquad (77)\end{aligned}$$

$$\begin{aligned}&\frac{V}{N}\sum_{\mathbf{k}\sigma}\left(\frac{\partial z_\sigma}{\partial p_\downarrow}\right)\left(\langle f^{\dagger}_{\mathbf{k}\sigma}c_{\mathbf{k}\sigma}\rangle+\mathrm{h.c.}\right)\\ &+2\sum_{\mathbf{k}\sigma}z_\sigma\left(\frac{\partial z_\sigma}{\partial p_\downarrow}\right)\varepsilon_{\mathrm{f}}\langle f^{\dagger}_{\mathbf{k}\sigma}f_{\mathbf{k}\sigma}\rangle = -2\left(\lambda^{(1)}-\lambda^{(2)}\right)p_\downarrow, \qquad (78)\end{aligned}$$

$$\begin{aligned}&\frac{V}{N}\sum_{\mathbf{k}\sigma}\left(\frac{\partial z_\sigma}{\partial d}\right)\left(\langle f^{\dagger}_{\mathbf{k}\sigma}c_{\mathbf{k}\sigma}\rangle+\mathrm{h.c.}\right)\\ &+2\sum_{\mathbf{k}\sigma}z_\sigma\left(\frac{\partial z_\sigma}{\partial d}\right)\varepsilon_{\mathrm{f}}\langle f^{\dagger}_{\mathbf{k}\sigma}f_{\mathbf{k}\sigma}\rangle = -2\left(\lambda^{(1)}-2\lambda^{(2)}\right)d, \qquad (79)\end{aligned}$$

$$\begin{aligned}&\frac{V}{N}\sum_{\mathbf{k}\sigma}\left(\frac{\partial z_\sigma}{\partial e}\right)\left(\langle f^{\dagger}_{\mathbf{k}\sigma}c_{\mathbf{k}\sigma}\rangle+\mathrm{h.c.}\right)\\ &+2\sum_{\mathbf{k}\sigma}z_\sigma\left(\frac{\partial z_\sigma}{\partial e}\right)\varepsilon_{\mathrm{f}}\langle f^{\dagger}_{\mathbf{k}\sigma}f_{\mathbf{k}\sigma}\rangle = -2\lambda^{(1)}e. \qquad (80)\end{aligned}$$

In this paper we consider the paramagnetic state and hence we assume $p_\uparrow=p_\downarrow=p$. The renormalization factor is then expressed as

$$z_\uparrow=z_\downarrow=z=\frac{\sqrt{1-2p^2}}{1-p^2}. \qquad (81)$$

Hereafter, we consider the case for $U=\infty$ for simplicity of analysis. Then we set $d=0$. By using Eq. (75), the derivative of the renormalization factor by p_σ and e can be expressed by only p, as follows:

$$\frac{\partial z_\sigma}{\partial p_\sigma} = \frac{\sqrt{1-2p^2}}{p\left(1-p^2\right)^{3/2}}, \qquad (82)$$

$$\frac{\partial z_\sigma}{\partial p_{-\sigma}} = \frac{\sqrt{1-2p^2}}{p\sqrt{1-p^2}}, \qquad (83)$$

$$\frac{\partial z_\sigma}{\partial e} = \frac{\sqrt{1-p^2}}{p^2}. \qquad (84)$$

Then, we end up by solving the mean-field equations of Eqs. (76), (77), and (79) for $\lambda^{(1)}$, $\lambda^{(2)}$, and p simultaneously with Eq. (2) for the chemical potential μ in the self-consistent manner. In these equations, the following expectation values are calculated as

$$\frac{1}{N}\sum_{\mathbf{k}\sigma}\langle f^{\dagger}_{\mathbf{k}\sigma}f_{\mathbf{k}\sigma}\rangle = -\frac{1}{\pi N}\sum_{\mathbf{k}\sigma}\int_{-\infty}^{\infty}d\varepsilon f(\varepsilon)\mathrm{Im}G^{\mathrm{ff\ R}}_{\mathbf{k}\sigma}(\varepsilon), \qquad (85)$$

$$\frac{1}{N}\sum_{\mathbf{k}\sigma}\langle c^{\dagger}_{\mathbf{k}\sigma}c_{\mathbf{k}\sigma}\rangle = -\frac{1}{\pi N}\sum_{\mathbf{k}\sigma}\int_{-\infty}^{\infty}d\varepsilon f(\varepsilon)\mathrm{Im}G^{\mathrm{cc\ R}}_{\mathbf{k}\sigma}(\varepsilon), \qquad (86)$$

$$\frac{1}{N}\sum_{\mathbf{k}\sigma}\langle f^{\dagger}_{\mathbf{k}\sigma}c_{\mathbf{k}\sigma}\rangle = -\frac{1}{\pi N}\sum_{\mathbf{k}\sigma}\int_{-\infty}^{\infty}d\varepsilon f(\varepsilon)\mathrm{Im}G^{\mathrm{fc\ R}}_{\mathbf{k}\sigma}(\varepsilon), \qquad (87)$$

Here, $G^{\mathrm{ff\ R}}_{\mathbf{k}\sigma}(\varepsilon)$, $G^{\mathrm{cc\ R}}_{\mathbf{k}\sigma}(\varepsilon)$, and $G^{\mathrm{fc\ R}}_{\mathbf{k}\sigma}(\varepsilon)$ are the retarded f-electron, conduction-electron, and off-diagonal green functions, respectively, which are given by

$$G^{\mathrm{ff\ R}}_{\mathbf{k}\sigma}(\varepsilon) = \tilde{a}^{\mathrm{ff}}_{-,\mathbf{k}}\tilde{G}^{-\mathrm{R}}_{\mathbf{k}\sigma}(\varepsilon)+\tilde{a}^{\mathrm{ff}}_{+,\mathbf{k}}\tilde{G}^{+\mathrm{R}}_{\mathbf{k}\sigma}(\varepsilon), \qquad (88)$$

$$G^{\mathrm{cc\ R}}_{\mathbf{k}\sigma}(\varepsilon) = \tilde{a}^{\mathrm{cc}}_{-,\mathbf{k}}\tilde{G}^{-\mathrm{R}}_{\mathbf{k}\sigma}(\varepsilon)+\tilde{a}^{\mathrm{cc}}_{+,\mathbf{k}}\tilde{G}^{+\mathrm{R}}_{\mathbf{k}\sigma}(\varepsilon), \qquad (89)$$

$$G^{\mathrm{fc\ R}}_{\mathbf{k}\sigma}(\varepsilon) = \tilde{a}^{\mathrm{fc}}_{-,\mathbf{k}}\tilde{G}^{-\mathrm{R}}_{\mathbf{k}\sigma}(\varepsilon)+\tilde{a}^{\mathrm{fc}}_{+,\mathbf{k}}\tilde{G}^{+\mathrm{R}}_{\mathbf{k}\sigma}(\varepsilon), \qquad (90)$$

respectively. In Eq. (88), $\tilde{a}^{\mathrm{ff}}_{-,\mathbf{k}}$ ($\tilde{a}^{\mathrm{ff}}_{+,\mathbf{k}}$) is the amplitude of the f-electron component in the lower (upper)-hybridized band at $\mathbf{k}$. In Eq. (89), $\tilde{a}^{\mathrm{cc}}_{-,\mathbf{k}}$ ($\tilde{a}^{\mathrm{cc}}_{+,\mathbf{k}}$) is the amplitude of the conduction-electron component in the lower (upper)-hybridized band at $\mathbf{k}$. These are given by

$$\tilde{a}^{\mathrm{ff}}_{\pm,\mathbf{k}}=\tilde{a}^{\mathrm{cc}}_{\mp,\mathbf{k}} = \frac{1}{2}\left(1\mp\frac{\varepsilon_{\mathbf{k}}-\tilde{\varepsilon}_{\mathrm{f}}}{\tilde{\Delta}_{\mathbf{k}}}\right). \qquad (91)$$

The weight factor $\tilde{a}^{\mathrm{fc}}_{-,\mathbf{k}}$ ($\tilde{a}^{\mathrm{fc}}_{+,\mathbf{k}}$) in the lower (upper) hybridized

band in Eq. (90) is given by

$$\tilde{a}^{\rm fc}_{-,\mathbf{k}} = -\frac{\tilde{V}}{\tilde{\Delta}_{\mathbf{k}}}, \tag{92}$$

$$\tilde{a}^{\rm fc}_{+,\mathbf{k}} = \frac{\tilde{V}}{\tilde{\Delta}_{\mathbf{k}}}. \tag{93}$$

Here, $\tilde{\Delta}_{\mathbf{k}}$ is given by

$$\tilde{\Delta}_{\mathbf{k}} = \sqrt{(\varepsilon_{\mathbf{k}} - \tilde{\varepsilon}_{\rm f})^2 + 4\tilde{V}^2}, \tag{94}$$

where $\tilde{\varepsilon}_{\rm f} \equiv \varepsilon_{\rm f} + \lambda^{(2)}$ and $\tilde{V} \equiv Vz$. We note that the relation $\tilde{a}^{\rm ff}_{\alpha,\mathbf{k}} + \tilde{a}^{\rm cc}_{\alpha,\mathbf{k}} = 1$ holds. In Eqs. (91) and (94), the f level $\varepsilon_{\rm f}$ and the hybridization strength V are replaced by $\tilde{\varepsilon}_{\rm f}$ and $\tilde{V}$ in Eqs. (30) and (29), respectively. The retarded Green function $\tilde{G}^{\alpha{\rm R}}_{\mathbf{k}\sigma}(\varepsilon)$ is given by

$$\tilde{G}^{\alpha{\rm R}}_{\mathbf{k}\sigma}(\varepsilon) = \frac{1}{\varepsilon - \tilde{E}^{(\alpha)}_{\mathbf{k}} + i\tilde{\Gamma}^{(\alpha)}_{\mathbf{k}}}, \tag{95}$$

where $\tilde{E}^{(\alpha)}_{\mathbf{k}}$ is given by

$$\tilde{E}^{\mp}_{\mathbf{k}} = \frac{\varepsilon_{\mathbf{k}} + \tilde{\varepsilon}_{\rm f}}{2} \mp \frac{\tilde{\Delta}_{\mathbf{k}}}{2}. \tag{96}$$

Here we consider the finite imaginary part of the self energy, $\tilde{\Gamma}^{(\alpha)}_{\mathbf{k}}$, in Eq. (95), as described in Eq. (72). In Sect. 2, Eq. (10) is expressed as

$$a^{\rm ff}_{\alpha,\mathbf{k}} = z_{\mathbf{k}} \left[1 + \frac{z_{\mathbf{k}} V^2}{(\varepsilon - \varepsilon_{\mathbf{k}})^2} \right]^{-1} \Bigg|_{\varepsilon = E^{\alpha *}_{\mathbf{k}}}. \tag{97}$$

In the present mean-field framework, the renormalization factor is expressed as z and the quasiparticle band is expressed as $\tilde{E}^{(\alpha)}_{\mathbf{k}}$. Hence, by setting $z_{\mathbf{k}}$ as z and $E^{\alpha *}_{\mathbf{k}}$ as $\tilde{E}^{(\alpha)}_{\mathbf{k}}$ in Eq. (97), $a^{\rm ff}_{\alpha,\mathbf{k}}$ is expressed as $z\tilde{a}^{\rm ff}_{\alpha,\mathbf{k}}$. Then, from Eq. (15), the damping rate of the quasiparticle is expressed as

$$\tilde{\Gamma}^{(\alpha)}_{\mathbf{k}} = z\tilde{a}^{\rm ff}_{\alpha,\mathbf{k}}\Gamma, \tag{98}$$

where Γ is defined as $\Gamma \equiv -{\rm Im}\Sigma^{\rm R}_{\mathbf{k}}(\mu) > 0$ in Eq. (72).

Hence, by using Eq. (95) as the Green function for quasiparticles, the ground-state properties of σ_{xx}, σ_{xy}/H, and the Hall coefficient will be discussed in the next Sect. on the basis of the exactly-derived formulas, Eq. (39) and Eq. (50).

As shown in Ref. 17, by calculating the vertex correction in the self energy and the total current consistently for the conductivity in the clean limit at finite temperatures, the total current $J_{\mathbf{k}\eta}$ has a finite value without diverging because of the presence of the Umklapp process in the periodic lattice in Eq. (23). In the present framework for the ground state ($T = 0$), we consider the self energy with the impurity scattering as in Eq. (69), which is consequently expressed as Eq. (72). As for the total current, the present framework corresponds to approximating the resultant $J_{\mathbf{k}\eta}$ as $v_{\mathbf{k}\eta}$ in Eq. (21).

The validity of this framework at least within approximating $J_{\mathbf{k}\eta}$ as $v_{\mathbf{k}\eta}$ is confirmed by comparing it with the finite-U result based on the Fermi-liquid theory in Sect. 2, which will be shown below (see also Appendix).

4.2 Numerical Results

On the basis of the theoretical framework described in the previous Sect., we calculate the conductivity in the periodic Anderson model on the square lattice. We consider

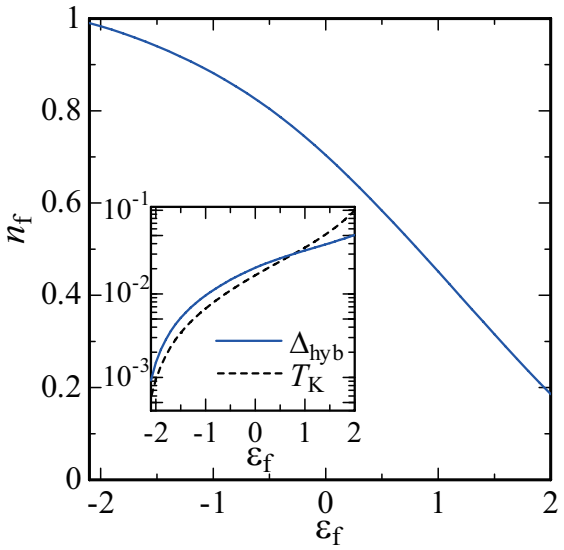

Fig. 2. (Color online) The $\varepsilon_{\rm f}$ dependence of the f-electron number per site for $t = 1$, $V = 0.3$, and $U = \infty$ at $\bar{n} = 7/4$ with $\Gamma = 10^{-3}$ calculated in the $N = 1200 \times 1200$ lattice sites. Inset: The $\varepsilon_{\rm f}$ dependence of $\Delta_{\rm hyb}$ (solid line) and $T_{\rm K}$ (dashed line).

the nearest-neighbor hopping for conduction electrons on the square lattice and the energy band is given by $\varepsilon_{\mathbf{k}} = -2t[\cos(k_x) + \cos(k_y)]$. As a typical parameter for heavy electrons, we set $t = 1$, $V = 0.3$, $U = \infty$ at the filling $\bar{n} = 7/4$. Hereafter, the transfer of conduction electrons is taken to be the energy unit of the parameters in the Hamiltonian, Eq. (73). The imaginary part of the f-electron self energy is set to be $\Gamma = 10^{-3}$ in Eq. (98) as a typical value. We solve the mean-field equations self-consistently at $T = 0$ in the several system sizes for $N = L_x^2$ with $L_x = 112$, 800, 1200, 1600, 1920, and 2240. Below we will show the results calculated on the lattice sites with $L_x = 1200$ unless otherwise noted.

4.2.1 *f-electron number per site and the characteristic energy*

Figure 2 shows the $\varepsilon_{\rm f}$ dependence of the f-electron number per site, $n_{\rm f}$. As $\varepsilon_{\rm f}$ increases, the crossover from the Kondo regime with $n_{\rm f} \approx 1$ in the deep-$\varepsilon_{\rm f}$ region to the valence-fluctuation[33] regime with $n_{\rm f} < 1$ in the shallow-$\varepsilon_{\rm f}$ region occurs in the ground state.

The characteristic energy scale of the present system, which is given by the hybridization gap $\Delta_{\rm hyb}$, is defined by the energy gap between the bottom of the upper hybridized band and the top of the lower hybridized band of quasiparticles:

$$\Delta_{\rm hyb} \equiv \tilde{E}^{+}_{\mathbf{k}=(0,0)} - \tilde{E}^{-}_{\mathbf{k}=(\pi,\pi)}. \tag{99}$$

Since we consider the filling of $\bar{n} = 7/4$ less than half filling, the Fermi level is located at the lower hybridized band. The Kondo temperature $T_{\rm K}$, which is the characteristic energy scale of the heavy-electron system, is defined as the energy difference between the renormalized f level and the Fermi level $T_{\rm K} \equiv \tilde{\varepsilon}_{\rm f} - \mu$ in the present mean-field framework. The inset of Fig. 2 shows that $\Delta_{\rm hyb}$ (solid line) roughly corresponds to $T_{\rm K}$ (dashed line), both of which well scale for $\varepsilon_{\rm f} \lesssim 0$.

To visualize the Fermi surface at $\bar{n} = 7/4$, we plot the spectral function $A_\alpha(\mathbf{k}, \varepsilon) \equiv -\frac{1}{\pi}{\rm Im}G^{\alpha{\rm R}}_{\mathbf{k}}(\varepsilon)$ for $\alpha = -$ and $\varepsilon = \mu$ in Fig. 3. Here we show the contour plot for $\varepsilon_{\rm f} = -4.0$ as a

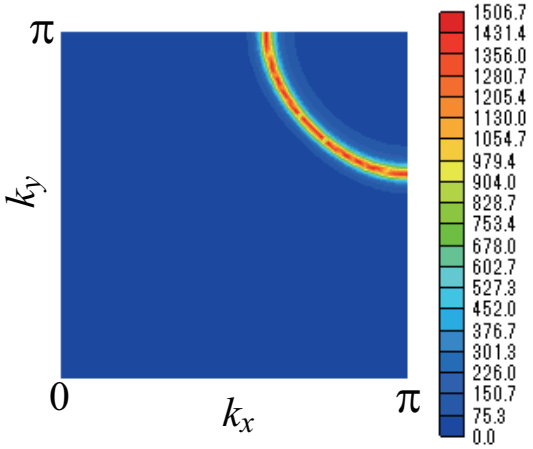

Fig. 3. (Color online) The contour plot of the spectral function $A_{-}(\mathbf{k},\mu) = -\mathrm{Im}[G^{-\mathrm{R}}_{\mathbf{k}}(\mu)]/\pi$ at $\bar{n} = 7/4$ for $t = 1$, $V = 0.3$, $\varepsilon_{\mathrm{f}} = -4.0$, and $U = \infty$ with $\Gamma = 10^{-3}$ calculated in the $N = 112 \times 112$ lattice sites.

typical case calculated in the $N = 112 \times 112$ lattice sites.

4.2.2 *Diagonal conductivity*

By using the mean-field solutions, the conductivity is calculated on the basis of Eq. (39) at $T = 0$. The ε_{f} dependence of σ_{xx} is shown in Fig. 4. In the deep-ε_{f} region, as ε_{f} increases, σ_{xx} shows a gradual increase which can be seen as almost constant behavior, while σ_{xx} shows a sharp increase in the shallow-ε_{f} region for $\varepsilon_{\mathrm{f}} \gtrsim 0$. The inset shows the ε_{f}-level dependence of the resistivity $\rho_{xx} = 1/\sigma_{xx}$.

To analyze the mechanism, we plot $\sigma^{(0)}_{xx}$ in Fig. 4, which is defined by

$$\sigma^{(0)}_{xx} = \frac{2e^2}{(2\pi)^2} \sum_{\mathbf{k}=\mathbf{k}_{\mathrm{F}}} \frac{\left(v^{\mathrm{c0}}_{\mathbf{k}x}\right)^2 \left(\tilde{a}^{\mathrm{cc}}_{-,\mathbf{k}}\right)^2}{\left|\nabla \tilde{E}^{-}_{\mathbf{k}}\right|} \tilde{\tau}^{-}_{\mathbf{k}} \, |\Delta\mathbf{k}| \,, \tag{100}$$

with $\tilde{\tau}^{-}_{\mathbf{k}} = \frac{1}{2\tilde{\Gamma}^{-}_{\mathbf{k}}}$. Here, the summation is taken over the Fermi wave vector $\mathbf{k}_{\mathrm{F}}$ and $|\Delta\mathbf{k}|$ is the length between each next $\mathbf{k}_{\mathrm{F}}$ point. This is the two-dimensional version of Eq. (59) in the lattice system. We see that the result almost coincides with σ_{xx}. This indicates that σ^{--}_{xx} in Eq. (40) gives the dominant contribution to σ_{xx} in Eq. (39) and the analysis with the small $\Gamma^{-}_{\mathbf{k}}$ in Eq. (55) is applicable to the parameter regime shown in Fig. 4. Since the velocity of the lower hybridized band $\tilde{\mathbf{v}}^{--}_{\mathbf{k}} \equiv \nabla \tilde{E}^{-}_{\mathbf{k}}$ is given by $\mathbf{v}^{--}_{\mathbf{k}} = \mathbf{v}^{\mathrm{c0}}_{\mathbf{k}} \tilde{a}^{\mathrm{cc}}_{-,\mathbf{k}}$ [see Eq. (43)], Eq. (100) can be expressed as

$$\sigma^{(0)}_{xx} = \frac{2e^2}{(2\pi)^2} \sum_{\mathbf{k}=\mathbf{k}_{\mathrm{F}}} \frac{\left(v^{\mathrm{c0}}_{\mathbf{k}x}\right)^2 \tilde{a}^{\mathrm{cc}}_{-,\mathbf{k}}}{\left|\mathbf{v}^{\mathrm{c0}}_{\mathbf{k}}\right| 2\tilde{\Gamma}^{-}_{\mathbf{k}}} \, |\Delta\mathbf{k}| \,. \tag{101}$$

This implies that the ratio of the conduction-electron weight factor $\tilde{a}^{\mathrm{cc}}_{-,\mathbf{k}_{\mathrm{F}}}$ and the damping rate $\tilde{\Gamma}^{-}_{\mathbf{k}_{\mathrm{F}}}$ determines the behavior of $\sigma^{(0)}_{xx}$. This gives essentially the same form as Eq. (16), which was formulated on the basis of the Fermi-liquid theory,[17] as shown in Appendix. This indicates the validity of the present formalism.

In order to clarify the ε_{f} dependence of $\tilde{\Gamma}^{-}_{\mathbf{k}}$ from Eq. (98) in detail, we plot in Fig. 5 the ε_{f} dependence of the renormalization factor z and the f-electron weight factor which is

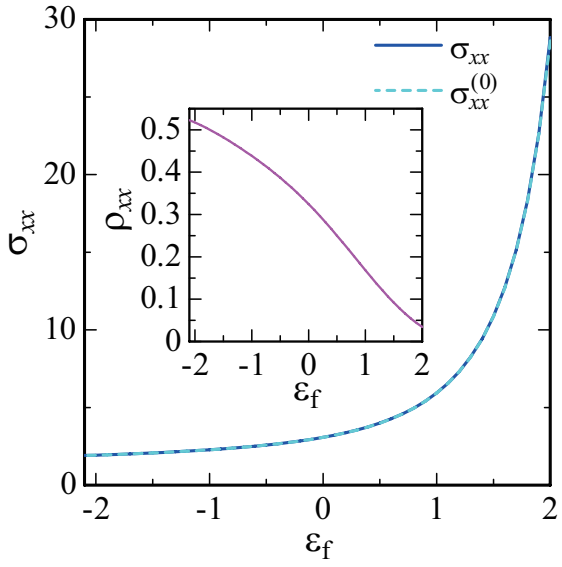

Fig. 4. (Color online) The ε_{f} dependence of the conductivity σ_{xx} (solid line) and $\sigma^{(0)}_{xx}$ (dashed line) for $t = 1$, $V = 0.3$, and $U = \infty$ at $\bar{n} = 7/4$ with $\Gamma = 10^{-3}$ is shown in the left axis, which is calculated in the $N = 1200 \times 1200$ lattice sites. We set $e = 1$. Inset shows the ε_{f}-level dependence of resistivity $\rho_{xx} = 1/\sigma_{xx}$.

averaged over the Fermi surface

$$\langle \tilde{a}^{\mathrm{ff}}_{-,\mathbf{k}_{\mathrm{F}}} \rangle_{\mathrm{av}} \equiv \frac{1}{N_{\mathbf{k}_{\mathrm{F}}}} \sum_{\mathbf{k}=\mathbf{k}_{\mathrm{F}}} \tilde{a}^{\mathrm{ff}}_{-,\mathbf{k}} \tag{102}$$

with $N_{\mathbf{k}_{\mathrm{F}}}$ being the number of the $\mathbf{k}_{\mathrm{F}}$ points. As ε_{f} increases, $\langle \tilde{a}^{\mathrm{ff}}_{-,\mathbf{k}_{\mathrm{F}}} \rangle_{\mathrm{av}}$ is kept to be almost 1 up to $\varepsilon_{\mathrm{f}} \sim 1$ and sharply decreases to zero for $\varepsilon_{\mathrm{f}} \gtrsim 1$.

The renormalization factor z approaches zero in the deep-ε_{f} limit due to strong correlation effect on f electrons with $n_{\mathrm{f}} \to 1$ (see Fig. 2). As ε_{f} increases, z increases gradually. The damping rate $\tilde{\Gamma}^{-}_{\mathbf{k}}$ given by the multiplication of $\tilde{a}^{\mathrm{ff}}_{-,\mathbf{k}}$ and z in Eq. (98) is averaged over the Fermi surface

$$\langle \tilde{\Gamma}^{-}_{\mathbf{k}_{\mathrm{F}}} \rangle_{\mathrm{av}} = \frac{1}{N_{\mathbf{k}_{\mathrm{F}}}} \sum_{\mathbf{k}=\mathbf{k}_{\mathrm{F}}} \tilde{\Gamma}^{-}_{\mathbf{k}}, \tag{103}$$

which shows a peak structure around $\varepsilon_{\mathrm{f}} \sim 2$ as shown in Fig. 5. An important result here is that $\langle \tilde{\Gamma}^{-}_{\mathbf{k}_{\mathrm{F}}} \rangle_{\mathrm{av}}$ is suppressed compared to $\Gamma = 10^{-3}$ in all the ε_{f} region since in both the large-ε_{f} and small-ε_{f} limits $\tilde{\Gamma}^{-}_{\mathbf{k}_{\mathrm{F}}}$ approaches zero and the peak value is bounded by the small Γ.

Figure 6 shows the ε_{f} dependence of the conduction-electron weight factor averaged over the Fermi surface

$$\langle \tilde{a}^{\mathrm{cc}}_{-,\mathbf{k}_{\mathrm{F}}} \rangle_{\mathrm{av}} \equiv \frac{1}{N_{\mathbf{k}_{\mathrm{F}}}} \sum_{\mathbf{k}=\mathbf{k}_{\mathrm{F}}} \tilde{a}^{\mathrm{cc}}_{-,\mathbf{k}}. \tag{104}$$

In Fig. 6, $\langle \tilde{\Gamma}^{-}_{\mathbf{k}_{\mathrm{F}}} \rangle_{\mathrm{av}}$ is also re-plotted for comparison. As ε_{f} increases, $\langle \tilde{a}^{\mathrm{cc}}_{-,\mathbf{k}_{\mathrm{F}}} \rangle_{\mathrm{av}}$ increases gradually in the deep-ε_{f} region, while it shows a sharp increase around $\varepsilon_{\mathrm{f}} \sim 1$. The gradual increase in $\langle \tilde{a}^{\mathrm{cc}}_{-,\mathbf{k}_{\mathrm{F}}} \rangle_{\mathrm{av}}$ and $\langle \tilde{\Gamma}^{-}_{\mathbf{k}_{\mathrm{F}}} \rangle_{\mathrm{av}}$ in the deep-ε_{f} region gives rise to cancellation of the effect of the mass renormalization[17] in Eq. (101), which causes the almost constant ε_{f} dependence of $\sigma^{(0)}_{xx}$. However, as ε_{f} increases to reach the shallow-ε_{f} region, $\varepsilon_{\mathrm{f}} \gtrsim 0$, i.e., so-called the "valence-fluctuation" regime, the cancellation does not work, where $a^{\mathrm{cc}}_{-,\mathbf{k}_{\mathrm{F}}}$ increases sharply

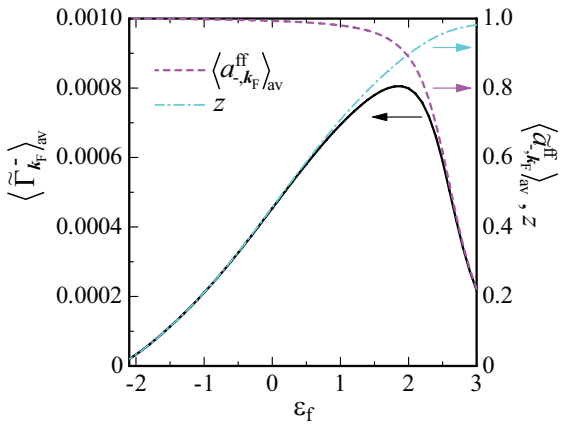

Fig. 5. (Color online) The ε_f dependence of the f-electron weight factor $\langle \tilde{a}^{ff}_{-,\mathbf{k}_F}\rangle_{av}$ (dashed line) and the renormalization factor z (dash-dotted line) for $t = 1$, $V = 0.3$, and $U = \infty$ at $\bar{n} = 7/4$ with $\Gamma = 10^{-3}$ is shown in the right axis, which is calculated in the $N = 1200 \times 1200$ lattice sites. The ε_f dependence of the imaginary part of the self energy $\langle \tilde{\Gamma}^{-}_{\mathbf{k}_F}\rangle_{av}$ is also plotted (solid line) in the left axis.

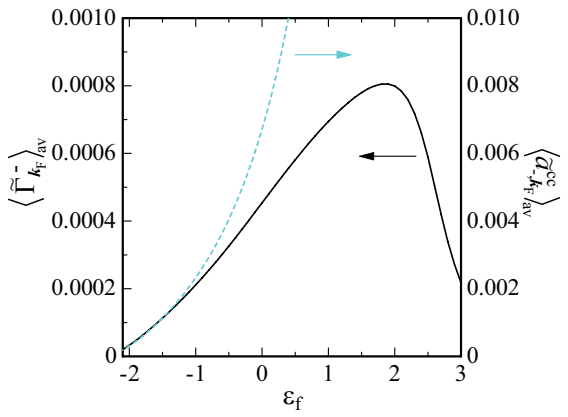

Fig. 6. (Color online) The ε_f dependence of the conduction-electron weight factor $\langle \tilde{a}^{cc}_{-,\mathbf{k}_F}\rangle_{av}$ (dashed line, right axis) and the imaginary part of the selfenergy $\langle \tilde{\Gamma}^{-}_{\mathbf{k}_F}\rangle_{av}$ (solid line, left axis) is shown, which is calculated for $t = 1$, $V = 0.3$, and $U = \infty$ at $\bar{n} = 7/4$ with $\Gamma = 10^{-3}$ in the $N = 1200 \times 1200$ lattice sites.

while $\tilde{\Gamma}^{-}_{\mathbf{k}_F}$ remains small. This imbalance is the reason why σ_{xx} shows a sharp increase in the valence-fluctuation regime for $\varepsilon_f \gtrsim 0$ in Fig. 4. This gives a natural explanation for the pressure dependence of the residual resistivity frequently observed in the Ce-based compounds and Yb-based compounds. The pressure dependence of the conductivity will be discussed in detail in Sect. 4.2.7.

The above result is obtained by using constant Γ in Eq. (72). As noted below Eq. (71), $\langle a^{ff}_{-,\mathbf{k}_F}\rangle_{av} N^*(\mu)$ can be expressed essentially by the bare quantities, which is on the order of $O(\pi V^2 N_{cF})^{-1}$. Hence, Γ defined in Eq. (72) has only weak-ε_f dependence. However, as shown in Fig. 5, the quantities related to renormalization factor, z and $\tilde{a}^{ff}_{-,\mathbf{k}}$ in Eq. (98), have strong ε_f dependence, which give the main contribution to the remarkable change of σ_{xx} when ε_f varies from the Kondo regime to the valence-fluctuation regime. Hence, present treatment using constant Γ is considered to capture the essence of the transport phenomena. As for the hybridization dependence, we have also performed the calculations of the ε_f dependence of σ_{xx} by inputting several values of Γ and confirmed that the main conclusion above does not change as far as the renormalized damping rate is far smaller than the hybridization gap. The Γ dependence and the V dependence will be discussed in Sect. 4.2.6 and Sect. 4.2.7, respectively.

4.2.3 Hall conductivity

The ε_f dependence of the Hall conductivity is shown in Fig. 7. The Hall conductivity σ_{xy}/H is calculated by using Eq. (50) at $T = 0$. As ε_f increases, in the deep-ε_f region σ_{xy}/H gradually increases, which can be seen as almost constant behavior, while it shows a sharp increase in the shallow-ε_f region for $\varepsilon_f \gtrsim 0$.

To analyze the mechanism, we plot $\sigma^{(0)}_{xy}/H$ in Fig. 7, which is defined by

$$\frac{\sigma^{(0)}_{xy}}{H} = -\frac{2e^3}{(2\pi)^2} \sum_{\mathbf{k}=\mathbf{k}_F} \frac{\left(v^{c0}_{\mathbf{k}x}\right)^2 \left(\frac{\partial v^{c0}_{\mathbf{k}y}}{\partial k_y}\right) \left(\tilde{a}^{cc}_{-,\mathbf{k}}\right)^3}{\left|\nabla \tilde{E}^{-}_{\mathbf{k}}\right|} (\tilde{\tau}^{-}_{\mathbf{k}})^2 \, |\Delta \mathbf{k}| \quad (105)$$

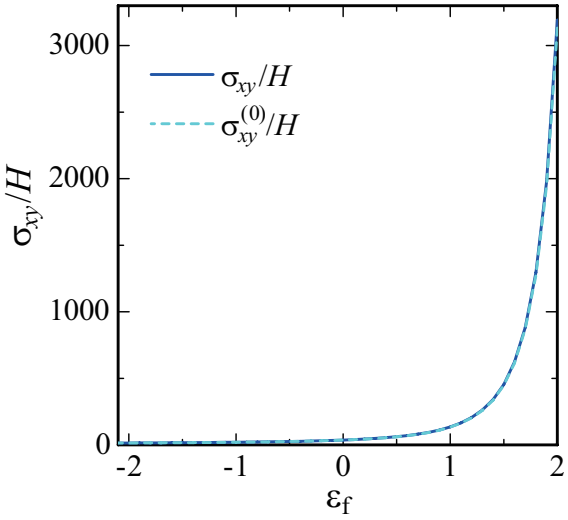

Fig. 7. (Color online) The ε_f dependence of the conductivity σ_{xy}/H (solid line) and $\sigma^{(0)}_{xy}/H$ (dashed line) for $t = 1$, $V = 0.3$, and $U = \infty$ at $\bar{n} = 7/4$ with $\Gamma = 10^{-3}$ is shown in the left axis, which is calculated in the $N = 1200 \times 1200$ lattice sites. We set $e = 1$.

dimensional version of Eq. (63) in the lattice system. We see that the result almost coincides with σ_{xy}/H. This indicates that σ^{--}_{xy}/H in Eq. (51) dominantly contributes to σ_{xy}/H in Eq. (50) and the analysis by the small $\tilde{\Gamma}^{-}_{\mathbf{k}} = \frac{1}{2\tilde{\tau}^{-}_{\mathbf{k}}}$ in Eq. (58) is applicable to the parameter regime shown in Fig. 7. By using the velocity of the lower hybridized band, $\tilde{\mathbf{v}}^{--}_{\mathbf{k}} = \nabla \tilde{E}^{-}_{\mathbf{k}} = \mathbf{v}^{c0}_{\mathbf{k}} a^{cc}_{-,\mathbf{k}}$, Eq. (105) can be expressed as

$$\frac{\sigma^{(0)}_{xy}}{H} = -\frac{2e^3}{(2\pi)^2} \sum_{\mathbf{k}=\mathbf{k}_F} \frac{\left(v^{c0}_{\mathbf{k}x}\right)^2 \left(\frac{\partial v^{c0}_{\mathbf{k}y}}{\partial k_y}\right) \left(\tilde{a}^{cc}_{-,\mathbf{k}}\right)^2}{\left|\mathbf{v}^{c0}_{\mathbf{k}}\right| \left(2\tilde{\Gamma}^{-}_{\mathbf{k}}\right)^2} |\Delta \mathbf{k}| \, . \quad (106)$$

In the right hand side, $(\tilde{a}^{cc}_{-,\mathbf{k}_F}/\tilde{\Gamma}^{-}_{\mathbf{k}_F})^2$ appears, which implies that the ratio $\tilde{a}^{cc}_{-,\mathbf{k}_F}/\tilde{\Gamma}^{-}_{\mathbf{k}_F}$ determines the behavior of $\sigma^{(0)}_{xy}/H$. As shown in Fig. 6, in the deep-ε_f region, $\tilde{a}^{cc}_{-,\mathbf{k}_F}/\tilde{\Gamma}^{-}_{\mathbf{k}_F}$ increases gradually, while it shows a sharp increase in the shallow-ε_f region for $\varepsilon_f \gtrsim 0$. Namely, cancellation of the effect of the mass

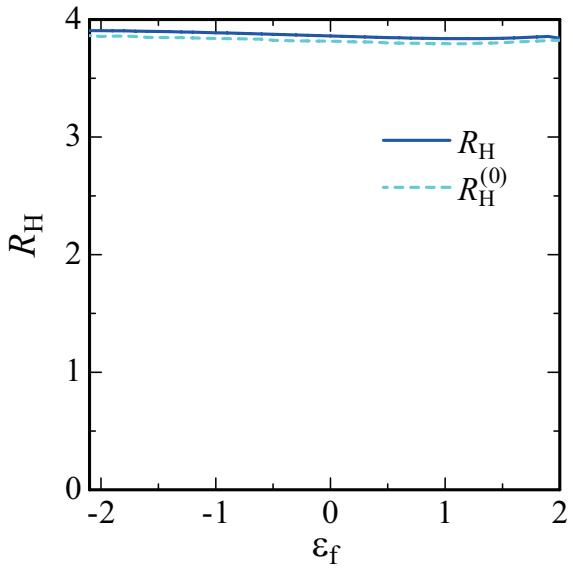

Fig. 8. (Color online) The $\varepsilon_{\rm f}$ dependence of the conductivity $R_{\rm H}$ (solid line) and $R_{\rm H}^{(0)}$ (dashed line) for $t = 1$, $V = 0.3$, and $U = \infty$ at $\bar{n} = 7/4$ with $\Gamma = 10^{-3}$ is shown in the left axis, which is calculated in the $N = 1200\times1200$ lattice sites. We set $e = 1$.

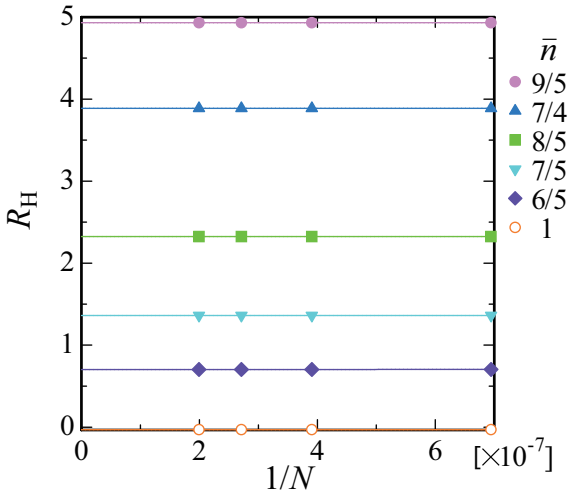

Fig. 9. (Color online) The system-size dependence of the Hall coefficient $R_{\rm H}$ for $t = 1$, $V = 0.3$, $\varepsilon_{\rm f} = -4.0$, and $U = \infty$ with $\Gamma = 10^{-3}$ at $\bar{n} = 1$ (open circle), 6/5 (filled diamond), 7/5 (filled inverted triangle), 8/5 (filled square), 7/4 (filled triangle), and 9/5 (filled circle). We set $e = 1$.

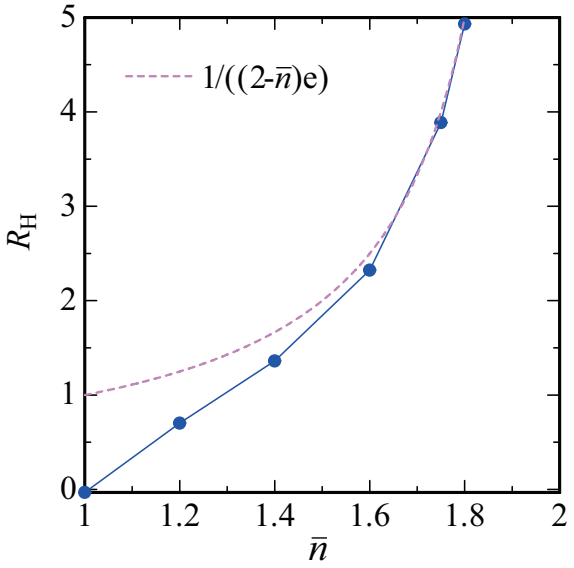

Fig. 10. (Color online) The filling dependence of the Hall coefficient $R_{\rm H}$ for $t = 1$, $V = 0.3$, $\varepsilon_{\rm f} = -4.0$, and $U = \infty$ with $\Gamma = 10^{-3}$ in the bulk limit ($N \to \infty$). The dashed line represents $1/((2-\bar{n})e)$. We set $e = 1$.

enhancement, i.e., $\tilde{a}^{\rm cc}_{-,\mathbf{k}_{\rm F}}/\tilde{\Gamma}^{-}_{\mathbf{k}_{\rm F}} \approx 1$, causes the almost constant behavior of σ_{xy}/H in the deep-$\varepsilon_{\rm f}$ region and the imbalance, i.e., $\tilde{a}^{\rm cc}_{-,\mathbf{k}_{\rm F}}/\tilde{\Gamma}^{-}_{\mathbf{k}_{\rm F}} \gg 1$, makes the sharp increase in σ_{xy}/H in the valence-fluctuation regime for $\varepsilon_{\rm f} \gtrsim 0$ in Fig. 7.

4.2.4 *Hall coefficient*

The $\varepsilon_{\rm f}$ dependence of the Hall coefficient is shown in Fig. 8. Here we set $e = 1$. The Hall coefficient $R_{\rm H} = \sigma_{xy}/(H\sigma_{xx}^2)$ (solid line) calculated by using Eqs. (39) and (50) shows a slight decrease as a function of $\varepsilon_{\rm f}$, exhibiting almost constant behavior. Namely, the sharp increase in σ_{xx} and σ_{xy}/H in the valence-fluctuation regime for $\varepsilon_{\rm f} \gtrsim 0$ in Fig. 4 and Fig. 7, respectively, cancel out each other in $R_{\rm H}$. To analyze this cancellation which occurs even in the valence-fluctuation regime, let us plot $R_{\rm H}^{(0)} = \sigma_{xy}^{(0)}/(H\sigma_{xx}^{(0)2})$ by the dashed line calculated by using Eqs. (100) and (105) in Fig. 8. We see that $R_{\rm H}^{(0)}$ also exhibits almost constant behavior. This is understood from expressions Eq. (100) and Eq. (105) since the factors of $\tilde{a}^{\rm cc}_{-,\mathbf{k}_{\rm F}}/\tilde{\Gamma}^{-}_{\mathbf{k}_{\rm F}}$ which appear in both $\sigma_{xx}^{(0)}$ and $\sigma_{xy}^{(0)}/H$ cancel out in $R_{\rm H}^{(0)}$. The close agreement between $R_{\rm H}$ and $R_{\rm H}^{(0)}$ indicates that the cancellation of the factors of $\tilde{a}^{\rm cc}_{-,\mathbf{k}_{\rm F}}/\tilde{\Gamma}^{-}_{\mathbf{k}_{\rm F}}$ actually occurs in $R_{\rm H}$, as was shown for the isotropic free-electrons in Eq. (68). However, in Fig. 8, the sign in $R_{\rm H}$ is positive and the magnitude is not expressed by the total filling as $1/(\bar{n}e) = 4/(7e)$, which are in contrast to the result to Eq. (68). These points will be analyzed below.

To figure out the filling dependence of $R_{\rm H}$, we calculate σ_{xx} and σ_{xy}/H for $1 \le \bar{n} < 2$ plausible to the heavy-electron state in several system sizes and extrapolate $R_{\rm H}$ to the bulk limit, $N = L_x^2 \to \infty$. Figure 9 shows $R_{\rm H}$ vs. $1/N$ for $\varepsilon_{\rm f} = -4.0$ at $\bar{n} = 1$, 6/5, 7/5, 8/5, 7/4, and 9/5. The system sizes used for the extrapolation are $N = L_x^2$ with $L_x = 1200$, 1600, 1920, and 2240.

The $\bar{n}$ dependence of $R_{\rm H}$ in the bulk limit is shown in Fig. 10. Note that the error bar by the least-square fit done for the system-size extrapolation is attached to each filled circle. The error bars are within the symbol sizes and invisible, indicating that the system size dependence does not matter in the $N \ge 1200$ lattice sites. Here, we also plot the Hall coefficient expressed by the hole density as $R_{\rm H}^{\rm hole} = \frac{1}{n_{\rm hole}e}$ with $\bar{n}_{\rm hole} \equiv 2 - \bar{n}$ by a dashed line (Note that we set $e = 1$). We can see that $R_{\rm H}$ approaches $R_{\rm H}^{\rm hole}$ as $\bar{n}$ approaches half filling, $\bar{n} = 2$. However, $R_{\rm H}$ approaches zero as $\bar{n}$ approaches 1, which shows a clear deviation from the dashed line. These results indicate that near the quarter filling, i.e., for $1 \le \bar{n} \lesssim 1.6$, $R_{\rm H}$ is not expressed simply by the hole density as $\frac{1}{n_{\rm hole}e}$.

4.2.5 *Curvature of the Fermi surface and Hall conductivity and Hall coefficient*

To understand the reason why $R_{\rm H}$ does not follow the simple relation $R_{\rm H} = 1/(\bar{n}_{\rm hole}e)$, we analyze σ_{xx}/H from the view

point of the curvature of the Fermi surface. In the single-band system constituted of a single orbital, it has been shown that σ_{xy}/H can be expressed by the angle between $\vec{v}_{\mathbf{k}}$ and the k_x axis within the Boltzmann transport theory[12–14] and the theory considering the vertex corrections.[24] In the present system, there exist two orbitals of f and conduction electrons, which form the lower and upper hybridized bands. Since the Fermi level is located at the lower hybridized band, the system is regarded as the single-band system at $T = 0$ in the small-$\tilde{\Gamma}^{--}_{\mathbf{k}}$ limit.

At sufficiently low temperatures in the small damping rate, σ^{--}_{xy}/H in Eq. (51) dominantly contributes to σ_{xy}/H in Eq. (50). Let us write Eq. (57) in the original form like Eq. (50) as

$$\sigma_{xy}/H = -\frac{e^3}{2V_0}\sum_{\mathbf{k}\sigma}\left(-\frac{\partial f(\tilde{E}^{--}_{\mathbf{k}})}{\partial \tilde{E}^{--}_{\mathbf{k}}}\right) \times \tilde{v}^{--}_{\mathbf{k}x}\left[\tilde{v}^{--}_{\mathbf{k}x}\left(\frac{\partial \tilde{v}^{--}_{\mathbf{k}y}}{\partial k_y}\right) - \tilde{v}^{--}_{\mathbf{k}y}\left(\frac{\partial \tilde{v}^{--}_{\mathbf{k}x}}{\partial k_y}\right)\right]\frac{2}{4(\tilde{\Gamma}^{--}_{\mathbf{k}})^2} \quad (107)$$

Here, by Eq. (43), the velocity of the lower hybridized band $\mathbf{v}^{--}_{\mathbf{k}} = \nabla \tilde{E}^{--}_{\mathbf{k}}$ in the present system for Eq. (73) is written as

$$\mathbf{v}^{--}_{\mathbf{k}} = \mathbf{v}^{c0}_{\mathbf{k}}\tilde{a}^{cc}_{-,\mathbf{k}} \equiv \tilde{\mathbf{v}}^{--}_{\mathbf{k}}. \quad (108)$$

Now we apply the formalism shown in Ref. 24 to Eq. (107). Here we describe it up to Eq. (116) below as the self-contained explanation although it was originally published in Ref. 24 [see Eq. (22) in Ref. 24].

For the subsequent discussion, we rewrite Eq. (107) as follows

$$\sigma_{xy}/H = -\frac{e^3}{2V_0}\sum_{\mathbf{k}\sigma}\left(-\frac{\partial f(\tilde{E}^{--}_{\mathbf{k}})}{\partial \tilde{E}^{--}_{\mathbf{k}}}\right)A^{--}_{xy}(\mathbf{k})\frac{2}{4(\tilde{\Gamma}^{--}_{\mathbf{k}})^2}, \quad (109)$$

by introducing

$$A^{--}_{xy}(\mathbf{k}) \equiv \tilde{v}^{--}_{\mathbf{k}x}\left[\tilde{v}^{--}_{\mathbf{k}x}\left(\frac{\partial \tilde{v}^{--}_{\mathbf{k}y}}{\partial k_y}\right) - \tilde{v}^{--}_{\mathbf{k}y}\left(\frac{\partial \tilde{v}^{--}_{\mathbf{k}x}}{\partial k_y}\right)\right]. \quad (110)$$

As shown in Ref. 20 [see Eq. (3.21) in Ref. 20], this can be rewritten in a simpler form as

$$\sigma_{xy}/H = -\frac{e^3}{4V_0}\sum_{\mathbf{k}\sigma}\left(-\frac{\partial f(\tilde{E}^{--}_{\mathbf{k}})}{\partial \tilde{E}^{--}_{\mathbf{k}}}\right)A^{--}_{\mathrm{s}}(\mathbf{k})\frac{2}{4(\tilde{\Gamma}^{--}_{\mathbf{k}})^2}, \quad (111)$$

where $A_{\mathrm{s}}(\mathbf{k})$ is defined as

$$A^{--}_{\mathrm{s}}(\mathbf{k}) = A^{--}_{xy}(\mathbf{k}) + A^{--}_{yx}(\mathbf{k}). \quad (112)$$

This can be expressed as[24]

$$A^{--}_{\mathrm{s}}(\mathbf{k}) = \tilde{v}^{--}_{\mathbf{k}x}(\vec{e}_z \times \tilde{\mathbf{v}}^{--}_{\mathbf{k}})\nabla\tilde{v}^{--}_{\mathbf{k}y} - \tilde{v}^{--}_{\mathbf{k}y}(\vec{e}_z \times \tilde{\mathbf{v}}^{--}_{\mathbf{k}})\nabla\tilde{v}^{--}_{\mathbf{k}x}, \quad (113)$$

$$= \left|\tilde{\mathbf{v}}^{--}_{\mathbf{k}}\right|\left(\tilde{\mathbf{v}}^{--}_{\mathbf{k}} \times \frac{\partial}{\partial k_{\parallel}}\tilde{\mathbf{v}}^{--}_{\mathbf{k}}\right)_z, \quad (114)$$

$$= \left|\tilde{\mathbf{v}}^{--}_{\mathbf{k}}\right| \cdot \left|\tilde{\mathbf{v}}^{--}_{\mathbf{k}}\right|^2\left(\frac{d\theta_{\tilde{\mathbf{v}}^{--}}(\mathbf{k})}{dk_{\parallel}}\right), \quad (115)$$

where $k_{\parallel}$ is the component of $\vec{k}$ along the vector $\vec{e}_{\parallel}(\mathbf{k}) = (\vec{e}_z \times \vec{\tilde{v}}^{--}_{\mathbf{k}})/\left|\tilde{\mathbf{v}}^{--}_{\mathbf{k}}\right|$, and tangential to the Fermi surface at $\mathbf{k}$ since $\tilde{\mathbf{v}}^{--}_{\mathbf{k}}$ is perpendicular to the Fermi surface. In Eq. (115), $\theta_{\tilde{v}^{--}(\mathbf{k})}$ is the angle between $\tilde{\mathbf{v}}^{--}_{\mathbf{k}}$ and the k_x axis.

By applying the similar derivation used in Eq. (63) to Eq. (111), $\sum_{\mathbf{k}}$ can be expressed by the line integral along the

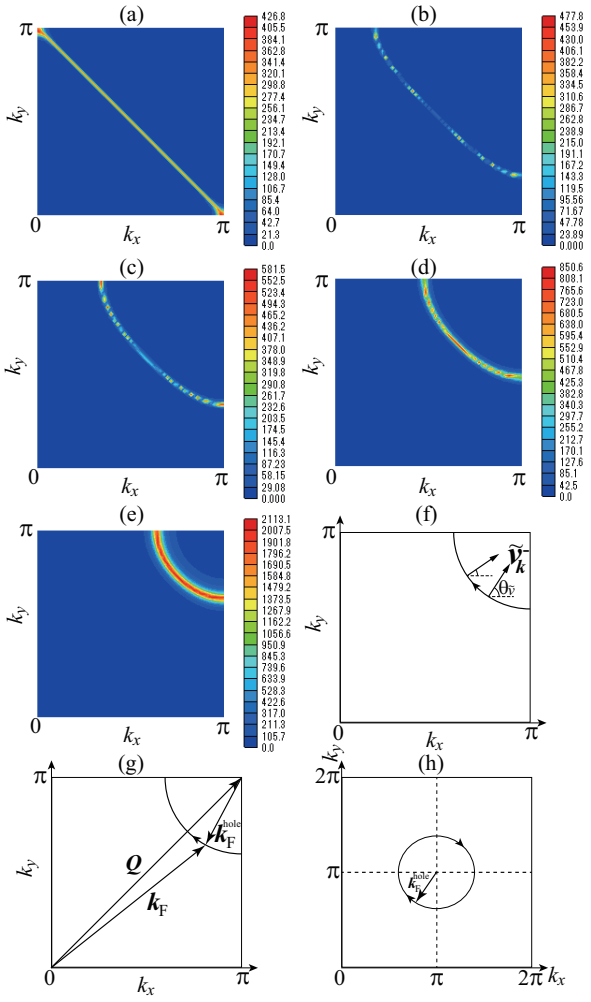

Fig. 11. (Color online) The contour plot of the spectral function $A_{-}(\mathbf{k},\mu) = -\mathrm{Im}[G^{\mathrm{R}}_{\mathbf{k}}(\mu)]/\pi$ at (a) $\bar{n} = 1$, (b) 6/5, (c) 7/5, (d) 8/5, and (e) 9/5 for $t = 1$, $V = 0.3$, $\varepsilon_{\mathrm{f}} = -4.0$, and $U = \infty$ with $\Gamma = 10^{-3}$ calculated in the $N = 112 \times 112$ lattice sites. (f) The velocity of the lower hybridized band $\tilde{\mathbf{v}}_{\mathbf{k}}$ on the Fermi surface $\mathbf{k} = \mathbf{k}_{\mathrm{F}}$. (g) The relation among $\mathbf{k}_{\mathrm{F}}$, $\mathbf{k}^{\mathrm{hole}}_{\mathrm{F}}$, and $\mathbf{Q} = (\pi,\pi)$, $\mathbf{k}_{\mathrm{F}} = \mathbf{Q} + \mathbf{k}^{\mathrm{hole}}_{\mathrm{F}}$. (h) The path for the line integral Eq. (117) along the Fermi surface.

Fermi surface in the present two-dimensional system. Then we have

$$\sigma_{xy}/H = -\frac{e^3}{4}\frac{2}{(2\pi)^2}\oint_{\mathrm{FS}} dk_{\parallel}\left|\tilde{\mathbf{v}}^{--}_{\mathbf{k}}\right|^2\left(\frac{d\theta_{\tilde{v}^{--}}(\mathbf{k})}{dk_{\parallel}}\right)\frac{2}{4(\tilde{\Gamma}^{--}_{\mathbf{k}})^2}, \quad (116)$$

where the $\mathbf{k}$ point moves counterclockwise along the Fermi surface in this line integral. Note that by Eq. (108) the mass renormalization factors appear as $(\tilde{a}^{cc}_{-,\mathbf{k}}/\tilde{\Gamma}^{--}_{\mathbf{k}})^2$ in the integrand, which cancel out in the deep-ε_{f} region as noted in Eq. (106).

To visualize the Fermi surface, we plot the spectral function $A_{\alpha}(\mathbf{k},\varepsilon) \equiv -\mathrm{Im}G^{\alpha\mathrm{R}}_{\mathbf{k}}(\varepsilon)/\pi$ for $\alpha = -$ and $\varepsilon = \mu$ at (a) $\bar{n} = 1$, (b) 6/5, (c) 7/5, (d) 8/5, and (e) 9/5 in Fig. 11. Here, set of parameters ($t = 1, V = 0.3, \varepsilon_{\mathrm{f}} = -4.0$, and $U = \infty$ with $\Gamma = 10^{-3}$) is the same as those in Fig. 9 and the results calculated in the $N = 112 \times 112$ lattice sites are shown.

At quarter filling, $\bar{n} = 1$, we see that $\theta_{\tilde{\mathbf{v}}^{--}_{\mathbf{k}}}(\mathbf{k})$ for example on the first quadrant does not change, since $\tilde{\mathbf{v}}^{--}_{\mathbf{k}_{\mathrm{F}}}$ is perpendicular to the Fermi surface, which makes $\theta_{\tilde{v}^{--}}(\mathbf{k}_{\mathrm{F}})$ be kept to be $\pi/4$. This gives rise to $d\theta_{\tilde{v}^{--}}(\mathbf{k})/dk_{\parallel} = 0$ in Eq. (116). Hence, it turns out that σ_{xy}/H and R_{H} as well become zero at $\bar{n} = 1$ at least

is shown to be almost zero although the spectral function is broaden near $\mathbf{k} = (0, \pi)$ and $(\pi, 0)$ in Fig. 11(a) because of the finite damping rate $\tilde{\Gamma}^{-}_{\mathbf{k}}$.

The reason why the sign of σ_{xy}/H and the resultant $R_{\rm H}$ become positive for $1 < \bar{n} < 2$ can be also understood from expression Eq. (116). As illustrated in Fig. 11(f), the angle $\theta_{\tilde{\mathbf{v}}^{-}}(\mathbf{k})$ becomes smaller as $k_{\parallel}$ moves along the Fermi surface. Namely, $d\theta_{\tilde{\mathbf{v}}^{-}}(\mathbf{k})/dk_{\parallel} < 0$ in Eq. (116) makes the sign of σ_{xy}/H be positive, and hence the positive Hall coefficient appears, $R_{\rm H} > 0$.

Furthermore, the reason why $R_{\rm H}$ approaches $1/((2-\bar{n})e)$ as $\bar{n}$ approaches half filling, 2, in Fig. 10 can be also understood on the basis of Eq. (116). As $\bar{n}$ approaches $\bar{n} = 2$, the form of the Fermi surface for holes approaches the circle around $\mathbf{k} = (\pi, \pi)$ as shown in Fig. 11(e). Hence, it is convenient to introduce the variable transformation $\mathbf{k}_{\rm F} = \mathbf{Q} + \mathbf{k}_{\rm F}^{\rm hole}$ with a constant shift $\mathbf{Q} = (\pi, \pi)$ in Eq. (116), as shown in Fig. 11(g). Then, Eq. (116) is expressed as

$$\sigma_{xy}/H = -\frac{e^3}{4}\frac{2}{(2\pi)^2}\oint_{\rm FS} dk_{\parallel}^{\rm hole}\left|\tilde{\mathbf{v}}^{-}_{\mathbf{k}}\right|^2\left(\frac{d\theta_{\tilde{\mathbf{v}}^{-}}(\mathbf{k})}{dk_{\parallel}^{\rm hole}}\right)\frac{2}{4(\tilde{\Gamma}^{-}_{\mathbf{k}})^2}. \quad (117)$$

When the Fermi surface is a circle, the integration can be easily performed as follows: Since the line integral in Fig. 11(h) is performed clockwise, the negative sign appears as $d\theta_{\tilde{\mathbf{v}}^{-}}(\mathbf{k})/dk_{\parallel}^{\rm hole} = -1/k_{\rm F}^{\rm hole}$. By using $\oint_{\rm FS} dk_{\parallel}^{\rm hole} = 2\pi k_{\rm F}$, we obtain

$$\sigma_{xy}/H = \frac{e^3}{4}\frac{1}{(2\pi)^2}2\pi k_{\rm F}^{\rm hole}\left(\tilde{v}^{-}_{k_{\rm F}^{\rm hole}}\right)^2\left(\frac{1}{k_{\rm F}^{\rm hole}}\right)\frac{1}{(\tilde{\Gamma}^{-}_{k_{\rm F}})^2}. \quad (118)$$

From Eq. (59) applied to the two-dimensional system, it can be shown that σ_{xx} for the hole Fermi surface with a circle shape is expressed as

$$\sigma_{xx} = \frac{e^2}{2\pi}k_{\rm F}^{\rm hole}\tilde{v}^{-}_{k_{\rm F}}\frac{1}{2\tilde{\Gamma}^{-}_{k_{\rm F}}}. \quad (119)$$

By Eqs. (118) and (119), the Hall coefficient is obtained as

$$R_{\rm H} = \frac{\sigma_{xy}}{H\sigma_{xx}^2} = \frac{1}{\bar{n}_{\rm hole}e}, \quad (120)$$

where the hole density is given by $\bar{n}_{\rm hole} = (k_{\rm F}^{\rm hole})^2/(2\pi)$ in the two-dimensional system. Then it is understandable that $R_{\rm H}$ is expressed by the hole density as $1/(\bar{n}_{\rm hole}e)$ with $\bar{n}_{\rm hole} \equiv 2 - \bar{n}$ as $\bar{n}$ approaches half filling, $\bar{n} = 2$, in Fig. 10.

4.2.6 *Damping-rate dependence*

So far, we have presented the results for the damping rate $\Gamma = 10^{-3}$ [see Eq. (72)] as a typical case. In this Subsect., we discuss the Γ dependence.

Figure 12 shows the $\varepsilon_{\rm f}$ dependence of the conductivity σ_{xx} for $t = 1$, $V = 0.3$, and $U = \infty$ at $\bar{n} = 7/4$ with (a) $\Gamma = 10^{-2}$, (b) 10^{-3}, and (c) 10^{-4} calculated in the $N = 1200 \times 1200$ lattice sites. Almost constant behavior in the deep-$\varepsilon_{\rm f}$ regime, i.e., Kondo regime, and sharp increase in the shallow-$\varepsilon_{\rm f}$ regime, i.e., valence-fluctuation regime appears in every case, although absolute value of σ_{xx} increases. As analyzed in Eq. (101), σ_{xx} is proportional to Γ^{-1}, which can be seen by comparing Fig. 12(b) with Fig. 12(c). However, the relation $\sigma_{xx} \propto \Gamma^{-1}$ does not seem to hold simply between Fig. 12(a) and Fig. 12(b). This indicates that the case of Fig. 12(a) cannot be regarded as the small-Γ regime where the analysis based on Eq. (101) is valid. This point will be more clearly seen when we calculate the Hall coefficient $R_{\rm H}$, which will be discussed in Fig. 14 below.

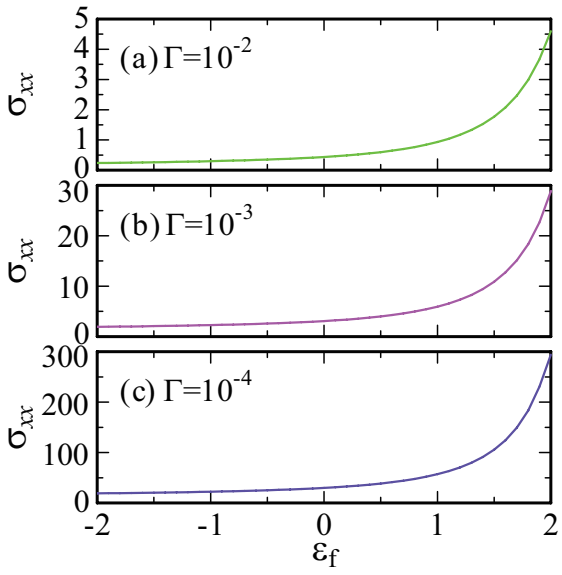

Fig. 12. (Color online) The $\varepsilon_{\rm f}$ dependence of the conductivity σ_{xx} for $t = 1$, $V = 0.3$, and $U = \infty$ at $\bar{n} = 7/4$ with (a) $\Gamma = 10^{-2}$, (b) 10^{-3}, and (c) 10^{-4} calculated in the $N = 1200 \times 1200$ lattice sites.

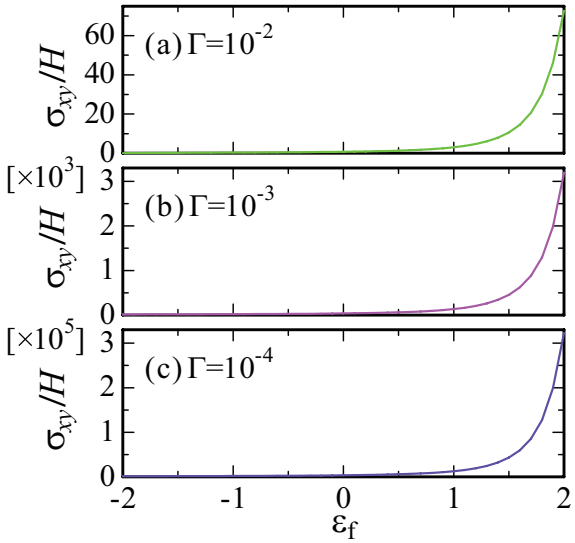

Fig. 13. (Color online) The $\varepsilon_{\rm f}$ dependence of the Hall conductivity σ_{xy}/H for $t = 1$, $V = 0.3$, and $U = \infty$ at $\bar{n} = 7/4$ with (a) $\Gamma = 10^{-2}$, (b) 10^{-3}, and (c) 10^{-4} calculated in the $N = 1200 \times 1200$ lattice sites.

Figure 13 shows the $\varepsilon_{\rm f}$ dependence of the Hall conductivity σ_{xy}/H for (a) $\Gamma = 10^{-2}$, (b) 10^{-3}, and (c) 10^{-4}. Almost constant behavior in the Kondo regime and sharp increase in the valence-fluctuation regime appears in every case. The relation $\sigma_{xy}/H \propto \Gamma^{-2}$, which is shown in Eq. (106), seems to hold between Figs. 13(b) and 13(c) but not between Figs. 13(a) and 13(b). As noted above, this is due to the fact that $\Gamma = 10^{-2}$ cannot be regarded as small Γ.

Figure 14 shows the $\varepsilon_{\rm f}$ dependence of the Hall coefficient $R_{\rm H}$ for $V = 0.3$ at $\bar{n} = 7/4$ for a series of damping rates due to impurity scattering; $\Gamma = 10^{-4}$ (dashed line), $\Gamma = 10^{-3}$ (solid line), and $\Gamma = 10^{-2}$ (dash-dotted line), which are calculated

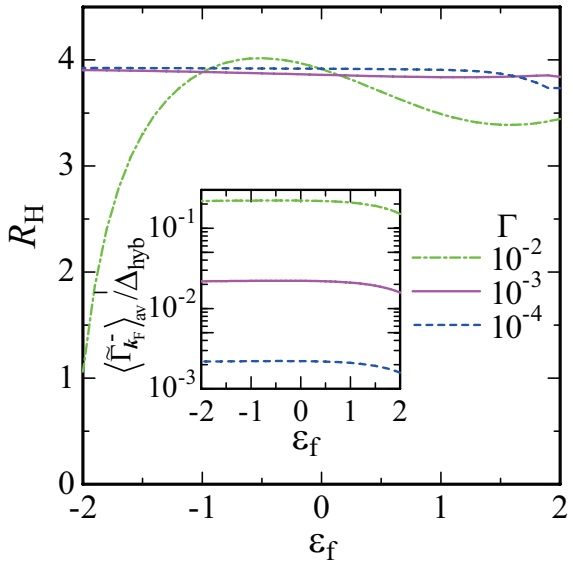

Fig. 14. (Color online) The ε_f dependence of the Hall coefficient R_H for $t = 1$, $V = 0.3$, and $U = \infty$ at $\bar{n} = 7/4$ with $\Gamma = 10^{-4}$ (dashed line), 10^{-3} (solid line), and 10^{-2} (dash-dotted line) calculated in the $N = 1200 \times 1200$ lattice sites. Inset: the ε_f dependence of $\langle\tilde{\Gamma}^-_{\mathbf{k}_F}\rangle_{av}/\Delta_{hyb}$. We set $e = 1$.

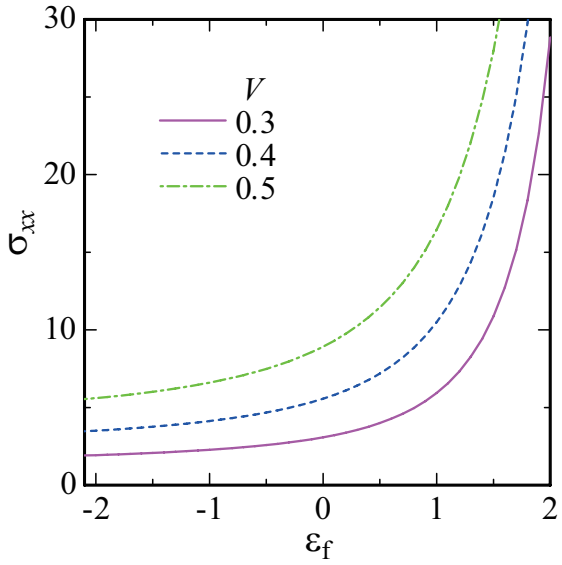

Fig. 15. (Color online) The ε_f dependence of the conductivity for $V = 0.3$ (solid line), 0.4 (dashed line) and 0.5 (dash-dotted line) at $t = 1$, $U = \infty$, $\bar{n} = 7/4$ with $\Gamma = 10^{-3}$ calculated in the $N = 1200 \times 1200$ lattice.

in the $N = 1200 \times 1200$ lattice sites. Almost constant ε_f dependence, $R_H \approx 1/(\bar{n}_{hole}e) = 4/e$, appears for $\Gamma = 10^{-4}$ and $\Gamma = 10^{-3}$. However, for $\Gamma = 10^{-2}$, R_H shows a visible deviation from the constant behavior.

To quantify the magnitude of the damping rate, in the inset of Fig. 14 we plot the ε_f dependence of the ratio of the damping rate averaged over the Fermi surface $\langle\tilde{\Gamma}^-_{\mathbf{k}_F}\rangle_{av}$ defined by Eq. (103) to Δ_{hyb} defined by Eq. (99). These results indicate that when the damping rate becomes comparable to about 10 % of the hybridization gap, the treatment of the small $\tilde{\Gamma}^-_{\mathbf{k}}$ discussed in Sect. 3.2 and also using Eqs. (100) and (105) are not justified. Namely, the contributions from the energies distant from the Fermi energy in Eq. (40) and Eq. (51) become relevant to σ_{xx} and σ_{xy}/H, respectively. For example, the downward deviation of R_H with $\Gamma = 10^{-2}$ seen in the deep-ε_f region in Fig. 14 reflects the tendency that the electron-like curvature of the $\mathbf{k}$ points in the $\varepsilon < \mu$ region of the lower hybridized band gives contributions with negative sign in σ_{xy}/H.

Hence, in the case that strong impurity scattering and/or high impurity density as well as the extraordinarily-strong correlation gives rise to a large damping rate which exceeds 10 % of the hybridization gap, R_H is not expressed simply by the hole density as $1/(\bar{n}_{hole}e)$ even near the half filling at $T = 0$. It is noted that not only the contributions distant from the Fermi energy to σ^{--}_{xx} in Eq. (40) and σ^{--}_{xy} in Eq. (51) but also the contributions other than the lower hybridized band are considered to play a significant role in σ_{xx} and σ_{xy} in such a case.

4.2.7 *Hybridization dependence and pressure dependence in Ce- and Yb-based compounds*

When pressure is applied to the Ce-based compounds, the anions surrounding the $Ce^{+3+\delta}$ ion approach the tail of the wavefunction of the 4f electron at the Ce site. This causes increase in the crystalline-electronic-field (CEF) level, i.e., ε_f increases. When pressure is applied to the Yb-based compounds, the negative ions surrounding the $Yb^{+3-\delta}$ ion approach, which also makes the 4f-electron level at the Yb site increase. Since Yb^{+3} contains $4f^{13}$ electrons, the hole picture is applied to the periodic Anderson model for the Yb-based systems. Hence, applying pressure makes the 4f-hole level ε_f decrease in Eq. (1).

In both the Ce- and Yb-based systems, the hybridization strength between f and conduction electrons is also expected to increase in general. In this subSect., we examine the hybridization dependence of the conductivity, the Hall conductivity, and the Hall coefficient.

In Fig. 15, we show ε_f dependence of σ_{xx} for $V = 0.3$ (solid line), 0.4 (dashed line) and 0.5 (dash-dotted line) with $\Gamma = 10^{-3}$, which is calculated in the $N = 1200 \times 1200$ lattice sites. We see that σ_{xx} shifts to larger values as V increases. As analyzed below Eq. (101), main contribution to σ_{xx} comes from $\tilde{a}^{cc}_{-,\mathbf{k}}/\tilde{\Gamma}^-_{\mathbf{k}}$ at the Fermi level. To clarify how hybridization strength affects this quantity, we plot the ε_f dependence of $\langle\tilde{\Gamma}^-_{\mathbf{k}_F}\rangle_{av}$ (solid line) and $\langle\tilde{a}^{cc}_{\mathbf{k}_F}\rangle_{av}$ (dashed line) for $V = 0.3$, 0.4 and 0.5 in Fig. 16. The result shows that the weight factor of conduction electrons $\langle\tilde{a}^{cc}_{\mathbf{k}_F}\rangle_{av}$ shifts to larger values remarkably as V increases while the damping rate of quasiparticles $\langle\tilde{\Gamma}^-_{\mathbf{k}_F}\rangle_{av}$ shows no marked enhancement. This can be understood from Eq. (98). Since the renormalized damping rate is expressed as multiplication of the renormalization factor z and the f-electron weight factor $\tilde{a}^{ff}_{-,\mathbf{k}}$, as V increases, increase in z and decrease in $\tilde{a}^{ff}_{-,\mathbf{k}}$ causes cancellation, giving rise to no remarkable enhancement of $\langle\tilde{\Gamma}^-_{\mathbf{k}_F}\rangle_{av}$. On the other hand, $\langle\tilde{a}^{cc}_{\mathbf{k}_F}\rangle_{av}$ increases as V increases since the weight of conduction electrons at the Fermi level increases by c-f hybridization as understandable from Eq. (91). Hence, it turns out that hybridization makes $\tilde{a}^{cc}_{-,\mathbf{k}_F}/\tilde{\Gamma}^-_{\mathbf{k}_F}$ increase, which results in increase in σ_{xx} in Fig. 15.

As for the Hall conductivity, the ε_f dependence of σ_{xy}/H for $V = 0.3$ (solid line), 0.4 (dashed line), and 0.5 (dash-dotted line) with $\Gamma = 10^{-3}$ is shown in Fig. 17, which is calculated in the $N = 1200 \times 1200$ lattice sites. As V increases,

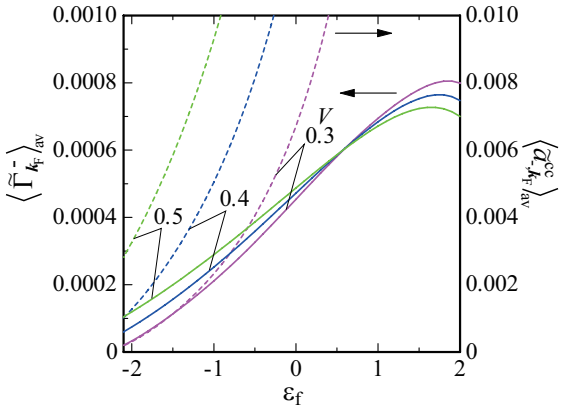

Fig. 16. (Color online) The ε_f dependence of the conduction-electron weight factor $\langle \tilde{a}^{cc}_{-,\mathbf{k}_F} \rangle_{av}$ (dashed line, right axis) and the imaginary part of the selfenergy $\langle \tilde{\Gamma}^-_{\mathbf{k}_F} \rangle_{av}$ (solid line, left axis) for $V = 0.3$, 0.4 and 0.5 at $t = 1$, $U = \infty$, $\bar{n} = 7/4$ with $\Gamma = 10^{-3}$ calculated in the $N = 1200 \times 1200$ lattice.

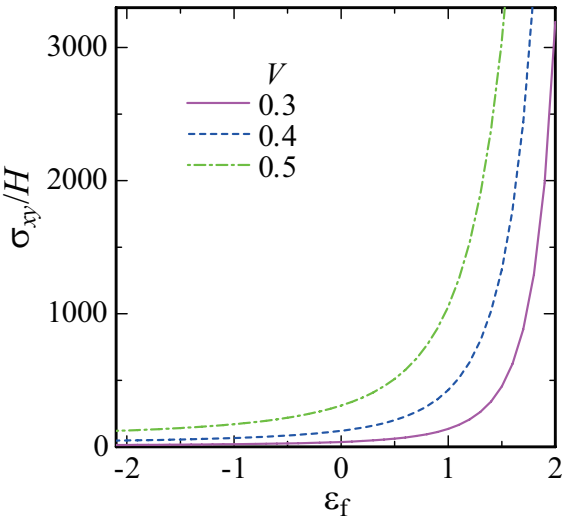

Fig. 17. (Color online) The ε_f dependence of the Hall conductivity for $V = 0.3$ (solid line), 0.4 (dashed line) and 0.5 (dash-dotted line) at $t = 1$, $U = \infty$, $\bar{n} = 7/4$ with $\Gamma = 10^{-3}$ calculated in the $N = 1200 \times 1200$ lattice.

σ_{xy}/H shifts to larger values, similarly to the case of σ_{xx}. This can be understood from Eq. (106). As analyzed below Eq. (106), main contribution to σ_{xy}/H comes from $(\tilde{a}^{cc}_{-,\mathbf{k}}/\tilde{\Gamma}^-_{\mathbf{k}})^2$ at the Fermi level. As shown in Fig. 16, $\tilde{a}^{cc}_{-,\mathbf{k}_F}/\tilde{\Gamma}^-_{\mathbf{k}_F}$ increases as V increases, which causes increase in σ_{xy}/H.

In Fig. 18, we plot the ε_f dependence of the Hall coefficient R_H for a series of hybridization strength; $V = 0.3$ (solid line), $V = 0.4$ (dashed line), and $V = 0.5$ (dash-dotted line) with $\Gamma = 10^{-3}$, which are calculated in the $N = 1200 \times 1200$ lattice sites. The result shows that even in the cases of $V = 0.4$ and $V = 0.5$ with increased hybridizations, the ε_f dependence of R_H remains almost the same as that for $V = 0.3$. This is because the factors $\tilde{a}^{cc}_{-,\mathbf{k}_F}/\tilde{\Gamma}^-_{\mathbf{k}_F}$ in σ_{xx} and σ_{xy}/H are canceled out each other in the expression of $R_H = \frac{\sigma_{xy}}{H\sigma^2_{xx}}$, as discussed in Sect. 4.2.4. This can be also understood from the results shown in Fig. 14. When V increases, the hybridization gap Δ_{hyb} increases while $\langle \tilde{\Gamma}^-_{\mathbf{k}_F} \rangle_{av}$ shows minor change as shown

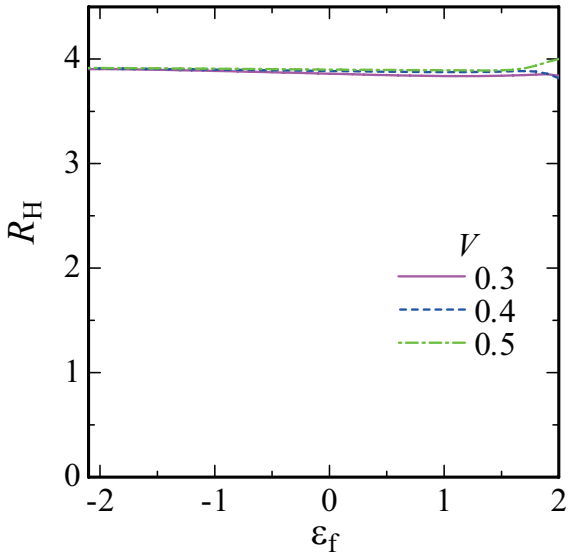

Fig. 18. (Color online) The ε_f dependence of the Hall coefficient R_H for $t = 1$ and $U = \infty$ at $\bar{n} = 7/4$ with $\Gamma = 10^{-3}$ calculated in the $N = 1200 \times 1200$ lattice sites. The results for $V = 0.3$ (solid line), 0.4 (dashed line), and 0.5 (dash-dotted line) are shown. We set $e = 1$.

in Fig. 16. Hence, the ratio $\langle \tilde{\Gamma}^-_{\mathbf{k}_F} \rangle_{av}/\Delta_{hyb}$ decreases. Then, the larger V makes the treatment of the small $\tilde{\Gamma}^-_{\mathbf{k}}$ works better in the calculations of σ_{xx}, σ_{xy}/H, and R_H, which reproduces the almost constant ε_f dependence of R_H.

In the Ce-based compounds, applying pressure makes ε_f and V increase in general. From the results shown in Figs. 4 and 13, and Figs. 7 and 15, σ_{xx} and σ_{xy}/H show gradual increase in the Kondo (deep-ε_f) regime and sharp increase in the valence-fluctuation (shallow-ε_f) regime as pressure increases. On the other hand, from the results shown in Figs. 8 and 16, almost unchanged R_H appears irrespective of the Kondo or valence-fluctuation regime under pressure as far as the system stays in the Fermi liquid. Hence, frequently observed behavior in the Ce-based compounds where the residual resistivity decreases gradually in the Kondo regime and drops sharply in the valence-fluctuation regime as pressure increases is naturally explained by the mechanism shown here.

In the Yb-based compounds, on the other hand, applying pressure makes V increase while ε_f in the hole picture decrease in general. Hence, pressure dependence of σ_{xx} and σ_{xy}/H depends on which factor is more effective. In case that the residual resistivity increases sharply in the valence-fluctuation regime and changes to the monotonic increase in the Kondo regime as pressure increases, it indicates that the effect of the ε_f dependence gives major contribution. In case that both effects of decreasing ε_f and increasing V are canceled each other, almost unchanged σ_{xx} and σ_{xy}/H as well as R_H are expected to appear under pressure.

5. Summary

We have derived exact formulas for σ_{xx} and σ_{xy} in the periodic Anderson model for $U = 0$, which give general expressions of the conductivities in the two-orbital systems with arbitrary band dispersions for $T = 0$ as well as finite temperatures. On the basis of the theoretical framework for the Fermi liquid based on these formulas, we have studied the ground-

the Hall coefficient in the periodic Anderson model with electron correlations on the square lattice, taking into account the effect of the weak local impurity scattering. The results obtained for the typical case where the Fermi level is located at the lower-hybridized band for the filling of $1 \leq \bar{n} < 2$ with the small damping rate are summarized as follows:

In the deep-$\varepsilon_{\rm f}$ region where $n_{\rm f} \gtrsim 0.8$, i.e., the Kondo regime, almost constant-$\varepsilon_{\rm f}$ dependence of σ_{xx} and σ_{xy}/H appears as a result of the cancellation of the mass renormalization factors. On the other hand, in the shallow-$\varepsilon_{\rm f}$ region, i.e., the valence-fluctuation regime with $n_{\rm f} \lesssim 0.8$, a sharp increase in σ_{xx} and σ_{xy}/H appears as $\varepsilon_{\rm f}$ increases. This is because the cancellation of the renormalization factors does not occur in the valence-fluctuation regime where the conduction-electron weight factor rapidly increases as $\varepsilon_{\rm f}$ increases while the f-electron damping rate remains to be suppressed.

On the contrary, the Hall coefficient $R_{\rm H}$ shows an almost constant $\varepsilon_{\rm f}$ dependence in the shallow-$\varepsilon_{\rm f}$ region as well as in the deep-$\varepsilon_{\rm f}$ region. This is because the renormalization factors expressed as the ratio of the conduction-electron weight factor to the damping rate for f electrons completely cancel out in the expression of $R_{\rm H}$. It is shown that $R_{\rm H}$ is expressed as $\frac{1}{\bar{n}_{\rm hole}e}$ with $\bar{n}_{\rm hole} \equiv 2 - \bar{n}$ as $\bar{n}$ approaches the half filling, $\bar{n} = 2$, while $R_{\rm H}$ approaches zero as $\bar{n}$ approaches the quarter filling, $\bar{n} = 1$. The reason is shown to be naturally understood from the curvatures of the Fermi surface.

We confirmed that the above conclusions hold at least for the small damping rate for f electrons where it is less than about 10 % of the hybridization gap, which roughly corresponds to the Kondo temperature. It is also confirmed that for the small damping rate the c-f hybridization dependence gives minor effects on the $\varepsilon_{\rm f}$ dependence of $R_{\rm H}$.

In this paper, we have concentrated on the ground-state properties of the typical periodic Anderson model for the Fermi liquid. Theoretically, it has been shown that the magnetically ordered phase generally appears in the deep-$\varepsilon_{\rm f}$ region with $n_{\rm f}$ being close to 1 in Eq. (1) if the counter effects such as the magnetic frustration are irrelevant.[34] In the systems where the inter-orbital Coulomb repulsion between the f electron and the conduction electron which contributes to the energy band located at the Fermi level has a certain magnitude, the quantum critical point (QCP) of the valence transition appears in the ground-state phase diagram.[1,2] As the magnitude of the c-f hybridization decreases, the QCP of the magnetic transition approaches the QCP of the valence transition and finally coincide each other where the enhanced critical valence fluctuation suppresses the magnetic order giving rise to the first-order magnetic transition.[34,35]

When we discuss the transport properties near the QCP of the phase transition such as the magnetic transition and the valence transition, the magnetic fluctuation[24,25] and the critical valence fluctuation[1,36] should be taken into account. Indeed, it was shown theoretically that near the QCP of the valence transition in the dirty system, the residual resistivity is enhanced considerably,[36] which explains the measurements in the $CeCu_2Ge_2$,[37] $CeCu_2Si_2$,[38] and $CeCu_2(Si_{1-x}Ge_x)_2$[39] systems. Hence, when the system approaches the QCP, such effects of the critical fluctuations give rise to additional effects on the results presented in this paper.

Acknowledgment

The authors are grateful to O. Narikiyo and Y. Fuseya for useful discussions on the transport theory by showing us their papers prior to publication. This work was supported by Grants-in-Aid for Scientific Research (No. 24540378 and No. 25400369) from the Japan Society for the Promotion of Science (JSPS). One of us (S.W.) was supported by JASRI (Proposal No. 0046 in 2012B, 2013A, 2013B, 2014A, 2014B, and 2015A).

Appendix: Renormalization factors in conductivity

In this Appendix, we show that the theoretical framework in Sect. 4.1 gives essentially the same analytic structure of the conductivity formulated on the basis of the Fermi-liquid theory in Sect. 2. Here we consider the case of $\varepsilon^{\rm f}_{\mathbf{k}} = \varepsilon_{\rm f}$ and $V_{\mathbf{k}} = V$ in Eq. (1) as discussed in Sect. 4.1. Let us start with the first line of Eq. (16):

$$\sigma^{(1)}_{xx} = \frac{e^2}{V_0}\sum_{\mathbf{k}}\int_{-\infty}^{\infty}\frac{d\varepsilon}{\pi}\left(-\frac{\partial f(\varepsilon)}{\partial\varepsilon}\right)\left|G^{\rm ff\ R}_{\mathbf{k}}(\varepsilon)\right|^2 v_{\mathbf{k}x}(\varepsilon)J_{\mathbf{k}x}(\varepsilon). \tag{A·1}$$

For $\Gamma^*_{\mathbf{k}} \ll T$, $\left|G^{\rm ff\ R}_{\mathbf{k}}(\varepsilon)\right|^2$ is evaluated as[16]

$$\left|G^{\rm ff\ R}_{\mathbf{k}}(\varepsilon)\right|^2 \approx 2\pi i\left(a^{\rm ff}_{-,\mathbf{k}}\right)^2\frac{\delta(\varepsilon - E^{-*}_{\mathbf{k}})}{i2\Gamma^*_{\mathbf{k}}}. \tag{A·2}$$

When the vertex correction in the total current is ignored in Eq. (21), the current is given by $J_{\mathbf{k}x}(\varepsilon) = v_{\mathbf{k}x}(\varepsilon)$. Then Eq. (A·1) leads to

$$\sigma^{(1)}_{xx} = \frac{e^2}{V_0}\sum_{\mathbf{k}}\left(-\frac{\partial f(E^{-*}_{\mathbf{k}})}{\partial E^{-*}_{\mathbf{k}}}\right)\left(a^{\rm ff}_{-,\mathbf{k}}\right)^2\frac{\left\{v_{\mathbf{k}x}(E^{-*}_{\mathbf{k}})\right\}^2}{\Gamma^*_{\mathbf{k}}}. \tag{A·3}$$

By using Eq. (11) and Eq. (17), the relation $\left(a^{\rm ff}_{-,\mathbf{k}}\right)^2\left\{v_{\mathbf{k}x}(E^{-*}_{\mathbf{k}})\right\}^2 = \left(a^{\rm cc}_{-,\mathbf{k}}\right)^2 v^{\rm c0\,2}_{\mathbf{k}x}$ holds. Hence, at sufficiently-low temperatures, $T \approx 0$, Eq. (A·3) is expressed as

$$\sigma^{(1)}_{xx} = \frac{e^2}{V_0}\sum_{\mathbf{k}}\delta\left(E^{-*}_{\mathbf{k}} - \mu\right)\frac{\left(a^{\rm cc}_{-,\mathbf{k}}\right)^2 v^{\rm c0\,2}_{\mathbf{k}x}}{\Gamma^*_{\mathbf{k}}}. \tag{A·4}$$

Since the factor $\left(a^{\rm cc}_{-,\mathbf{k}}\right)^{-1}$ arises from the delta function, $\delta(E^{-*}_{\mathbf{k}} - \mu)$ [see Eq. (101)], the factor $a^{\rm cc}_{-,\mathbf{k}}/\Gamma^*_{\mathbf{k}}$ finally appears in Eq. (A·4). This is the same as Eq. (101). This confirms the validity of the framework described in Sect. 4.1.

1) K. Miyake and S. Watanabe, J. Phys. Soc. Jpn. **83**, 061006 (2014).
2) S. Watanabe and K. Miyake, Phys. Rev. Lett. **105**, 186403 (2010).
3) T. Kagayama, G. Oomi, H. Takahashi, N. Mōri, Y. Ōnuki, and T. Komatsubara, Phys. Rev. B **44**, 7690 (1990).
4) T. Kagayama and G. Oomi, J. Phys. Soc. Jpn. **65**, Suppl. B 42 (1996).
5) S. Raymond and D. Jaccard, J. Low. Temp. Phys. **120**, 107 (2000).
6) K. Alami-Yadri, H. Wilhelm, and D. Jaccard, Solid State Commun. **108**, 279 (1998).
7) G. Knebel, D. Braithwaite, G. Lapertot, P. C. Canfield, and J. Flouquet, J. Phys.: Condens. Matter **13**, 10935 (2001).
8) H. Q. Yuan, M. Nicklas, Z. Hossain, C. Geibel, and F. Steglich, Phys. Rev. B **74**, 212403 (2006).
9) K. Matsubayashi, Y. Saiga, T. Matsumoto, and Y. Uwatoko, J. Phys.: Conference Series **150**, 042117 (2009).
10) F. Honda, S. Yasui, S. Yoshiuchi, T. Takeuchi, R. Settai, and Y. Ōnuki, J. Phys. Soc. Jpn. **79**, 083709 (2010).
11) S. K. Kim, M. S. Torikachvili, S. L. Bud'ko, and P. C. Canfield, Phys.

12) J. M. Ziman, *Electrons and Phonons* (Clarendon, Oxford, 1960).
13) M. Tsuji, J. Phys. Soc. Jpn. **13**, 979 (1958).
14) N. P. Ong, Phys. Rev. B **43**, 193 (1991).
15) R. Kubo, J. Phys. Soc. Jpn. **12**, 570 (1957).
16) G. M. Éliashbelg, Sov. Phys. JETP **14**, 886 (1962).
17) K. Yamada and K. Yosida, Prog. Theor. Phys. **76**, 621 (1986).
18) H. Fukuyama, H. Ebisawa, and Y. Wada, Prog. Theor. Phys. **42**, 494 (1969).
19) H. Fukuyama, Prog. Theor. Phys. **42**, 1284 (1969).
20) H. Kohno and K. Yamada, Prog. Theor. Phys. **80**, 623 (1988).
21) G. Baym and L. P. Kadanoff, Phys. Rev. **124**, 287 (1961).
22) G. Baym, Phys. Rev. **127**, 1391 (1962).
23) N. E. Bickers and S. R. White, Phys. Rev. B **47**, 6069 (1993).
24) H. Kontani, K. Kanki, and K. Ueda, Phys. Rev. B **59**, 14723 (1999).
25) H. Kontani, Rep. Prog. Phys. **71**, 026501 (2008).
26) O. Narikiyo, arXiv:1112.1513.
27) O. Narikiyo, arXiv:1203.0127.
28) Y. Fuseya, M. Ogata, and H. Fukuyama, J. Phys. Soc. Jpn. **84**, 012001 (2015).
29) N. W. Ashcroft and N. D. Mermin, *Solid State Physics* Chapter 8 (Thomson Learning, 1976).
30) A. A. Abrikosov, L. P. Gorkov, and I. E. Dzyaloshinski, *Methods of Quantum Field Theory in Statistical Physics* (Dover Books on Physics, 1975).
31) K. Miyake and H. Kohno, J. Phys. Soc. Jpn. **74**, 254 (2005).
32) G. Kotliar and A. Ruckenstein, Phys. Rev. Lett. **57**, 1362 (1986).
33) In this paper, we refer to the valence-fluctuation regime as the parameter region where $n_{\rm f} < 1$ is realized. In a series of the papers published by the present authors focusing on the quantum critical point of the valence transition (VQCP),[1)] we have used the mixed-valence (MV) regime to express the parameter region with $n_{\rm f} < 1$ since near the VQCP, the critical valence fluctuation is enhanced so that it has been necessary to avoid the confusion between the (ordinary) valence-fluctuation and the critical valence fluctuation. In the present paper, we restrict ourselves to the Fermi-liquid ground state. Hence, we use the valence-fluctuation regime instead of using the MV regime following the standard usage at present.
34) S. Watanabe and K. Miyake, J. Phys. Soc. Jpn. **79**, 033706 (2010).
35) S. Watanabe and K. Miyake, J. Phys.: Condens. Matter **23**, 094217 (2011).
36) K. Miyake and H. Maebashi, J. Phys. Soc. Jpn. **71**, 1007 (2002).
37) D. Jaccard, H. Wilhelm, K. Alami-Yadri, and E. Vargoz, Physica B **259-261**, 1 (1999).
38) A. T. Holmes, D. Jaccard, and K. Miyake, Phys. Rev. B **69**, 024508 (2004).
39) H. Q. Yuan, F. M. Groshe, M. Deppe, C. Geibel, G. Sparn, and F. Steglich, Science **302**, 2104 (2003).